PERGAMON

International Journal of Solids and Structures 38 (2001) 2573–2596

INTERNATIONAL JOURNAL OF SOLIDS and STRUCTURES

www.elsevier.com/locate/ijsolstr

# Some hybrid variational methods for linear electroelasticity problems

Agostino Antonio Cannarozzi, Francesco Ubertini *

*DISTART-Scienza delle Costruzioni, Università di Bologna, Viale Risorgimento 2, 40136 Bologna, Italy*

Received 29 October 1999; in revised form 18 April 2000

**Abstract**

Two methods for linear electroelastic analysis are presented, both supported by a variational formulation of hybrid type for stresses. In the first formulation, the field variables are stress and density of electric flux, and mechanical and electrical equilibria are satisfied a priori in the field. In the second formulation, the field variables are stress and electric potential, and mechanical equilibrium and electrical compatibility are satisfied a priori in the field. In both cases, the remaining field and boundary conditions are met weakly. Two finite element models are developed and their performance is examined and compared with the one of the compatible finite element approach in some test cases reported in the literature. © 2001 Elsevier Science Ltd. All rights reserved.

*Keywords:* Electroelasticity; Variational method; Hybrid model; Finite element

## 1. Introduction

The electroelastic behavior of materials is a topic of specific interest in solid mechanics as well as in structural engineering. Indeed, the state variables of mechanical and electrical nature are coupled in the constitutive law of an electroelastic body, since an electric field produces a deformation (electrostrictive effect) as well as a deformation a polarization state affects (piezoelectric effect) – see for example Eringen and Maugin (1990) and Ikeda (1996). In other words, an energy transfer takes place from electrical to mechanical energy, and vice versa. This feature makes an electroelastic structure able to adapt depending on the electrical or mechanical operating conditions, and several displays as control moduli (e.g. Gandhi and Thompson, 1992), piezoelectric motors (Carotenuto et al., 1998), etc. can be built by employing electroelastic materials.

Due to the theoretical and applicative aspects mentioned above, a continuative attention is devoted to electroelasticity problems in literature, both in formulating suited structural models and related methods of solutions (recent contributions are by Nicotra (1998), dell'Isola and Vidoli (1998), Nicotra and Podio Guidugli (1998) and Vidoli and Batra (1998)) and in implementing exact, analytical solutions for specific problems (see in particular Ray et al. (1992, 1993), Heyliger (1994), Bisegna and Maceri (1996),

* Corresponding author. Fax: +39-051-209-3495.
*E-mail address:* francesco.ubertini@mail.ing.unibo.it (F. Ubertini).

0020-7683/01/$ - see front matter 
PII: S0020-7683(00)00171-2

Kapuria et al. (1997) and Heyliger (1997)). These solutions are of interest to assess the accuracy of approximate methods of analysis, which are needed for solving most of the actual problems. Nevertheless, numerical solutions can also be suitable for benchmark comparisons.

In the above direction, a variational formulation of the problem can be of interest not only as a formal contribution, but also as a consistent support for developing a general and convenient method of analysis. A variational principle for linear electroelasticity necessarily recalls an analogous principle in elasticity. Indeed, the variational principle in displacement and electric potential presented earlier in the literature by Tiersten (1967, 1969), EerNisse (1967) and Holland and EerNisse (1968) is similar to Hamilton's principle and, of course, to the one of minimum potential energy. Four variational principles, corresponding to the four versions of the electroelastic energy were outlined by Zhang (1985). Each principle involves as variables, a function chosen between displacement and stress, and a function chosen between electric potential and electric flux density. In each principle, the variables fulfill the relevant equations of the boundary value problem as essential conditions. The extension of the Hu–Washizu and Hellinger–Reissner mixed principles is due to Yang (1992), for both static and dynamic cases. Finally, a long list of functionals for variational statements is given by Bisegna and Maceri (1998). On the side of the numerical solution procedures, the compatible finite element approach, i.e. the approach based on displacement and electric potential interpolation, seems to be universally followed – see the early papers of Allik and Hughes (1970) and Oden and Kelley (1971), the more recent paper of Lerch (1990), and the papers of Lee and Saravanos (1997) and Wang et al. (1999) for a comprehensive list of references. Recently, a different approach which anticipates some contents of this paper has been proposed by the authors (Cannarozzi and Ubertini, 1999).

In this paper, two distinct variational versions of the electroelasticity problem are exposed. Both are related to the minimum, modified complementary energy principle for the elastic part. In the first version, the field variables are stress and electric flux density. Mechanical equilibrium and electrical equilibrium are fulfilled a priori in the field, and compatibility and boundary conditions are met weakly. In the second version, the field variables are stress and electric potential, mechanical equilibrium and electrical compatibility are fulfilled a priori in the field, and the other field and boundary conditions are met weakly. The exposition is done with regard to a three-dimensional body for the sake of generality and because a three-dimensional description is often required for practical transducer applications, but the specialization to whatever structural model is obviously possible. Each formulation supports a finite element method of analysis where the elastic part is of hybrid type for stress (Pian, 1973), while the electrical part is of hybrid type for electric flux density in the first formulation, and of compatible type in the second one. The first method involves stress and electric flux density as variables in the element, and displacement and electric potential at the interelement, hence it allows direct evaluation and control for all the quantities of the problem. The second method is rather an improvement of the standard, compatible approach for what concerns stress analysis. In both cases, the greater computational burden seems to be rewarded by a superior overall accuracy in the results.

Passing to the details of the exposition, in Section 2 the energy functions at the basis of the two methods and the related constitutive equations are deduced, and the equilibrium and compatibility equations of the problem are recalled. The variational formulations involved are exposed in Section 3, and the related models are developed and discussed in Section 4, together with the finite element implementation. Some numerical tests are presented in Section 5 and the performances of the proposed approaches is accounted for. Some final considerations end the paper.

## 2. Governing equations

Reference is made to a body which occupies the closed and bounded domain $\bar{B}$ of the euclidean three-dimensional point space $\mathscr{E}$. The vector space associated to $\mathscr{E}$ is denoted by $\mathscr{V}$, $\{\mathbf{e}_i\} = \{\mathbf{e}_1, \mathbf{e}_2, \mathbf{e}_3\}$ is an

orthonormal basis of $\mathscr{V}$, and $(\mathbf{o};\mathbf{e}_1,\mathbf{e}_2,\mathbf{e}_3)$ is a cartesian reference frame for $\mathscr{E}$, with origin $\mathbf{o}$. The components of a vector $\mathbf{v}\in\mathscr{V}$ with respect to the assumed basis are denoted by $\{v_i\}$ and the coordinates of a point $\mathbf{x}$ of $\mathscr{E}$ are denoted by $\{x_i\}-i=1,...,3$. The inner part of $\bar{B}$ is denoted by $B$ and its boundary by $\partial B$, $B\cup\partial B=\bar{B}$. The measure of $B$ is $V$ and the measure of $\partial B$ is $S$.

The variables which describe the state of the body are the displacement vector $\mathbf{u}$ and the electric potential $\phi$, functions of $\mathbf{x}$ in $\bar{B}$, the symmetric strain tensor $\mathbf{E}$ and stress tensor $\mathbf{S}$, the electric field vector $\mathbf{e}$ and the electric flux density vector $\mathbf{d}$, functions of $\mathbf{x}$ in $B$. Traction and electric flux density through a surfacic element of unit normal vector $\mathbf{n}$ are denoted by $\mathbf{t}$, $\mathbf{t}=\mathbf{S}\mathbf{n}$, and $d$, $d=\mathbf{d}\cdot\mathbf{n}$, respectively. The domain $\bar{B}$ is admitted to assume outward normal vector almost everywhere on $\partial B$.

The distributed load $\mathbf{b}$ and the distributed electric charge $\gamma$ are prescribed in $B$. The boundary $\partial B$ is split into four parts: $\partial B_u$, $\partial B_s$ and $\partial B_\phi$, $\partial B_d$, such that $\partial B_u\cup\partial B_s=\partial B_\phi\cup\partial B_d=\partial B$, $\partial B_u\cap\partial B_s=\partial B_\phi\cap\partial B_d=\emptyset$. The values $\bar{\mathbf{u}}$ and $\bar{\mathbf{t}}$ are prescribed for displacement $\mathbf{u}$ on $\partial B_u$ and traction $\mathbf{t}$ on $\partial B_s$, respectively, and the values $\bar{\phi}$ and $\bar{d}$ are prescribed for the electric potential $\phi$ on $\partial B_\phi$ and for the density of electric charge on $\partial B_d$, respectively. All these quantities are assumed to be independent of time (electrostatic problem).

The context of the linear theory of electroelasticity is adopted (Eringen and Maugin, 1990). The state of the body is governed by the following relationships.

*Constitutive equations.* Due to the presence of the four inner variables: $\mathbf{E}$, $\mathbf{S}$, $\mathbf{e}$ and $\mathbf{d}$, four equivalent versions of the electroelastic constitutive equations are possible depending on the choice of the independent variables (see in particular Berlincourt et al. (1964) and Ikeda (1996)). Each version can be derived from a specific state function.

The constitutive equations in terms of strain and electric field are derived from the electric enthalpy function

$$\varphi(\mathbf{E},\mathbf{e})=\tfrac{1}{2}\mathbf{C}\mathbf{E}\cdot\mathbf{E}-\tfrac{1}{2}\mathbf{k}\mathbf{e}\cdot\mathbf{e}-\mathbf{c}\mathbf{E}\cdot\mathbf{e}, \tag{1}$$

and read

$$\mathbf{S}=\partial\varphi/\partial\mathbf{E}=\mathbf{C}\mathbf{E}-\mathbf{c}^{\mathrm{t}}\mathbf{e}, \tag{2}$$

$$\mathbf{d}=-\partial\varphi/\partial\mathbf{e}=\mathbf{c}\mathbf{E}+\mathbf{k}\mathbf{e}, \tag{3}$$

where $\mathbf{C}$ is the fourth-order tensor of elastic stiffness at constant electric field, $\mathbf{k}$ is the second-order permittivity tensor at constant strain, and $\mathbf{c}$ is the third-order electroelastic coupling tensor, all independent of $\mathbf{E}$ and $\mathbf{e}$. Tensors $\mathbf{C}$ and $\mathbf{k}$ are symmetric and positive definite, and tensor $\mathbf{c}$ is such that the product $\mathbf{c}^{\mathrm{t}}\mathbf{a}$ is a second-order symmetric tensor for each vector $\mathbf{a}$, being $\mathbf{c}^{\mathrm{t}}$ the transpose of $\mathbf{c}$ defined by $\mathbf{A}\cdot\mathbf{c}^{\mathrm{t}}\mathbf{a}=\mathbf{c}\mathbf{A}\cdot\mathbf{a}$, with $\mathbf{A}$ second-order symmetric tensor.

The Legendre transformation (Sewell, 1987) of $\varphi$ with all the variables active is the mechanical enthalpy function

$$\pi(\mathbf{S},\mathbf{d})=\varphi-\mathbf{E}\cdot\mathbf{S}-\mathbf{e}\cdot\mathbf{d}=\tfrac{1}{2}\mathbf{H}\mathbf{S}\cdot\mathbf{S}+\tfrac{1}{2}\mathbf{X}\mathbf{d}\cdot\mathbf{d}-\mathbf{h}\mathbf{S}\cdot\mathbf{d}, \tag{4}$$

and the related constitutive equations read

$$\mathbf{E}=-\partial\pi/\partial\mathbf{S}=\mathbf{H}\mathbf{S}+\mathbf{h}^{\mathrm{t}}\mathbf{d}, \tag{5}$$

$$\mathbf{e}=\partial\pi/\partial\mathbf{d}=-\mathbf{h}\mathbf{S}+\mathbf{X}\mathbf{d}, \tag{6}$$

where

$$\mathbf{H} = \left(\mathbf{C} + \mathbf{c}^{\mathrm{t}}\mathbf{k}^{-1}\mathbf{c}\right)^{-1}, \qquad \mathbf{h} = \mathbf{k}^{-1}\mathbf{c}\mathbf{H}, \qquad \mathbf{X} = \mathbf{k}^{-1} - \mathbf{k}^{-1}\mathbf{c}\mathbf{H}\mathbf{c}^{\mathrm{t}}\mathbf{k}^{-1}. \tag{7}$$

The electroelastic moduli of this version seem better suited to be obtained through direct measurements (Berlincourt et al., 1964). In this case, the moduli for the other versions are derived in turn.

The Legendre transformation of $\varphi$ with variables $\mathbf{E}$ and $\mathbf{S}$ active is the enthalpy function

$$\psi(\mathbf{S}, \mathbf{e}) = \varphi - \mathbf{E}\cdot\mathbf{S} = -\tfrac{1}{2}\mathbf{H}^{e}\mathbf{S}\cdot\mathbf{S} - \tfrac{1}{2}\mathbf{k}^{s}\mathbf{e}\cdot\mathbf{e} - \mathbf{h}\mathbf{S}\cdot\mathbf{e} \tag{8}$$

with the subsequent constitutive equations

$$\mathbf{E} = -\partial\psi/\partial\mathbf{S} = \mathbf{H}^{e}\mathbf{S} + \mathbf{g}^{\mathrm{t}}\mathbf{e}, \tag{9}$$

$$\mathbf{d} = -\partial\psi/\partial\mathbf{e} = \mathbf{g}\mathbf{S} + \mathbf{k}^{s}\mathbf{e}, \tag{10}$$

where

$$\mathbf{H}^{e} = \mathbf{C}^{-1}, \qquad \mathbf{g} = \mathbf{c}\mathbf{C}^{-1}, \qquad \mathbf{k}^{s} = \mathbf{k} + \mathbf{c}\mathbf{C}^{-1}\mathbf{c}^{\mathrm{t}}. \tag{11}$$

Tensors $\mathbf{H}$, $\mathbf{X}$, $\mathbf{H}^{e}$ and $\mathbf{k}^{s}$ are positive definite and tensors $\mathbf{h}$ and $\mathbf{g}$ have the same property of $\mathbf{c}$.

Functions $\pi$ and $\psi$ are directly involved in this work.

*Compatibility equations.* The strain–displacement and electric field–electric potential relationships, and the relevant boundary conditions are

$$\mathbf{E} = \operatorname{symgrad}\mathbf{u} \quad \text{in } B, \tag{12}$$

$$\mathbf{e} = -\operatorname{grad}\phi \quad \text{in } B, \tag{13}$$

$$\mathbf{u} = \bar{\mathbf{u}} \quad \text{on } \partial B_u, \tag{14}$$

$$\phi = \bar{\phi} \quad \text{on } \partial B_\phi. \tag{15}$$

*Equilibrium equations.* The mechanical and electrical balance equations are

$$\operatorname{div}\mathbf{S} + \mathbf{b} = \mathbf{0} \quad \text{in } B, \tag{16}$$

$$\operatorname{div}\mathbf{d} - \gamma = 0 \quad \text{in } B, \tag{17}$$

$$\mathbf{S}\mathbf{n} = \bar{\mathbf{t}} \quad \text{on } \partial B_s, \tag{18}$$

$$\mathbf{d}\cdot\mathbf{n} = -\bar{d} \quad \text{on } \partial B_d. \tag{19}$$

The differential operators above are related via the bilinear (Gauss–Green) identities

$$\int_B \mathbf{v}\cdot\operatorname{div}\mathbf{W}\,\mathrm{d}V = -\int_B \mathbf{W}\cdot\operatorname{symgrad}\mathbf{v}\,\mathrm{d}V + \int_{\partial B}\mathbf{v}\cdot\mathbf{W}\mathbf{n}\,\mathrm{d}S, \tag{20}$$

$$\int_B v\operatorname{div}\mathbf{w}\,\mathrm{d}V = -\int_B \mathbf{w}\cdot\operatorname{grad}v\,\mathrm{d}V + \int_{\partial B} v\mathbf{n}\cdot\mathbf{w}\,\mathrm{d}S, \tag{21}$$

where $v$ is a function of $\mathbf{x}$, and $\mathbf{v}$, $\mathbf{w}$ and $\mathbf{W}$ are two vectors and a symmetric tensor of sufficiently regular functions of $\mathbf{x}$.

## 3. Variational formulation

Two variational formulations are given. The first one is based on the mechanical enthalpy function (4). As the inner variables meet a priori mechanical and electrical equilibrium in $B$, and weakly the other conditions, this formulation is referred to as fully hybrid formulation. The second one is based on the enthalpy function (8) and the inner variables meet a priori mechanical equilibrium and electrical compatibility in $B$, thus it is referred to as hybrid stress formulation (Pian, 1973).

### 3.1. Fully hybrid formulation

A variational counterpart of the problem described in the previous Section is based on the functional (Cannarozzi and Ubertini, 1999)

$$\Pi(\mathbf{S},\mathbf{d},\mathbf{u},\phi) = \int_B \pi(\mathbf{S},\mathbf{d})\,\mathrm{d}V + \int_{\partial B_s} (\mathbf{S}\mathbf{n}-\bar{\mathbf{t}})\cdot\mathbf{u}\,\mathrm{d}S + \int_{\partial B_u} \mathbf{S}\mathbf{n}\cdot\bar{\mathbf{u}}\,\mathrm{d}S + \int_{\partial B_d} (\mathbf{d}\cdot\mathbf{n}+\bar{d})\,\phi\,\mathrm{d}S + \int_{\partial B_\phi} \mathbf{d}\cdot\mathbf{n}\,\bar{\phi}\,\mathrm{d}S, \tag{22}$$

concave in $\mathbf{S}$ and convex in $\mathbf{d}$, see Eq. (4). The domain of functional $\Pi$ is the cartesian product of the sets of functions $\mathbf{S}$ and $\mathbf{d}$ which satisfy equilibrium conditions (16) and (17) in $B$, respectively, and of the sets of functions $\mathbf{u}$ and $\phi$ which are continuous on $\partial B_s$ and $\partial B_d$, respectively. The first variation of $\Pi$ yields

$$\delta\Pi = \int_B \big(-\mathbf{H}\mathbf{S}\cdot\delta\mathbf{S} - \mathbf{h}^{\mathrm{t}}\mathbf{d}\cdot\delta\mathbf{S} + \mathbf{X}\mathbf{d}\cdot\delta\mathbf{d} - \mathbf{h}\mathbf{S}\cdot\delta\mathbf{d}\big)\mathrm{d}V + \int_{\partial B_s} \mathbf{u}\cdot\delta\mathbf{S}\mathbf{n}\,\mathrm{d}S + \int_{\partial B_u} \bar{\mathbf{u}}\cdot\delta\mathbf{S}\mathbf{n}\,\mathrm{d}S + \int_{\partial B_d} \phi\,\mathbf{n}\cdot\delta\mathbf{d}\,\mathrm{d}S + \int_{\partial B_\phi} \bar{\phi}\,\mathbf{n}\cdot\delta\mathbf{d}\,\mathrm{d}S + \int_{\partial B_s} (\mathbf{S}\mathbf{n}-\bar{\mathbf{t}})\cdot\delta\mathbf{u}\,\mathrm{d}S + \int_{\partial B_d} (\mathbf{d}\cdot\mathbf{n}+\bar{d})\,\delta\phi\,\mathrm{d}S, \tag{23}$$

where the variations $\delta\mathbf{S}$ and $\delta\mathbf{d}$ are submitted to the equilibrium conditions in the homogeneous form:

$$\mathrm{div}\,\delta\mathbf{S} = \mathbf{0}, \tag{24}$$

$$\mathrm{div}\,\delta\mathbf{d} = 0. \tag{25}$$

Let $\mathbf{v}$ denote a vector of functions of $\mathbf{x}$, and $v$ a function of $\mathbf{x}$. The term

$$-\int_B \mathrm{div}\,\delta\mathbf{S}\cdot\mathbf{v}\,\mathrm{d}V - \int_B v\,\mathrm{div}\,\delta\mathbf{d}\,\mathrm{d}V,$$

which is identically null, is added to functional $\delta\Pi$, and the application of identities (20) and (21), for sufficiently regular functions $\mathbf{S}$, $\mathbf{d}$, $\mathbf{u}$, $\phi$, $\mathbf{v}$ and $v$, yields

$$\delta\Pi = \int_B \big[\big(\mathrm{symgrad}\,\mathbf{v} - \mathbf{H}\mathbf{S} - \mathbf{h}^{\mathrm{t}}\mathbf{d}\big)\cdot\delta\mathbf{S} + (\mathrm{grad}\,v - \mathbf{h}\mathbf{S} + \mathbf{X}\mathbf{d})\cdot\delta\mathbf{d}\big]\mathrm{d}V - \int_{\partial B_s} (\mathbf{v}-\mathbf{u})\cdot\delta\mathbf{S}\mathbf{n}\,\mathrm{d}S - \int_{\partial B_u} (\mathbf{v}-\bar{\mathbf{u}})\cdot\delta\mathbf{S}\mathbf{n}\,\mathrm{d}S - \int_{\partial B_d} (v-\phi)\mathbf{n}\cdot\delta\mathbf{d}\,\mathrm{d}S - \int_{\partial B_\phi} (v-\bar{\phi})\mathbf{n}\cdot\delta\mathbf{d}\,\mathrm{d}S + \int_{\partial B_s} (\mathbf{S}\mathbf{n}-\bar{\mathbf{t}})\cdot\delta\mathbf{u}\,\mathrm{d}S + \int_{\partial B_d} (\mathbf{d}\cdot\mathbf{n}+\bar{d})\,\delta\phi\,\mathrm{d}S. \tag{26}$$

The variational equation

$$\delta\Pi = 0 \quad \forall(\delta\mathbf{S},\delta\mathbf{d},\delta\mathbf{u},\delta\phi) \tag{27}$$

generates the necessary and sufficient stationary conditions for functional $\Pi$ on the set of functions $\mathbf{S}$ and $\mathbf{d}$ which fulfill Eqs. (16) and (17):

$$\operatorname{symgrad}\mathbf{v} - \mathbf{HS} - \mathbf{h}^{\mathrm{t}}\mathbf{d} = \mathbf{0} \quad \text{in } B, \tag{28}$$

$$\operatorname{grad} v - \mathbf{hS} + \mathbf{Xd} = \mathbf{0} \quad \text{in } B, \tag{29}$$

$$\mathbf{v} - \mathbf{u} = \mathbf{0} \quad \text{on } \partial B_s, \tag{30}$$

$$\mathbf{Sn} - \bar{\mathbf{t}} = \mathbf{0} \quad \text{on } \partial B_s, \tag{31}$$

$$\mathbf{v} - \bar{\mathbf{u}} = \mathbf{0} \quad \text{on } \partial B_u, \tag{32}$$

$$v - \phi = 0 \quad \text{on } \partial B_d, \tag{33}$$

$$\mathbf{d}\cdot\mathbf{n} + \bar{d} = 0 \quad \text{on } \partial B_d, \tag{34}$$

$$v - \bar{\phi} = 0 \quad \text{on } \partial B_\phi. \tag{35}$$

It follows from the above equations that if $\Pi$ is stationary there exists a vector $\mathbf{v}$ which identifies with displacement $\mathbf{u}$, and a function $v$ which identifies with potential $\phi$, so that the compatibility equations and the equilibrium equations (18) and (19) are fulfilled. Hence, the point of stationary of functional $\Pi$ corresponds to the solution of the electroelastic problem. The exposed formulation can be alternatively derived from the mixed principle of Hellinger–Reissner's type presented by Yang (1992).

The requirements of regularity for functions $\mathbf{S}$ and $\mathbf{d}$ can be relaxed on a finite number of interfaces in $B$ for finite element expansions. Domain $B$ is subdivided into $E$ non-overlapping open subdomains $B_e$, $e = 1, ..., E$, with boundary $\partial B_e$, $\bar{B}_e = B_e \cup \partial B_e$, $\cup_e \bar{B}_e = \bar{B}$. The intersection, if any, between $\partial B_e$ and a part of $\partial B$ is denoted by $\partial B_{ue}$, $\partial B_{\phi e}$, $\partial B_{se}$, $\partial B_{de}$, according to the relevant part of $\partial B$. The interdomain between two subdomains is denoted by $\varrho_j$, $j = 1, ..., m$. Displacement $\mathbf{u}$ and potential $\phi$ are assumed to be continuous on the interdomain, whereas continuity of tractions and electric flux density through the interface of two contiguous subdomains, $(\mathbf{Sn})_j^+$ and $(\mathbf{d}\cdot\mathbf{n})_j^+$, $(\mathbf{Sn})_j^-$ and $(\mathbf{d}\cdot\mathbf{n})_j^-$, is relaxed. Hence, functional (22) becomes

$$\begin{aligned}\Pi_D(\mathbf{S},\mathbf{d},\mathbf{u},\phi) = \sum_e \Bigg[ &\int_{B_e} \pi(\mathbf{S},\mathbf{d})\,\mathrm{d}V + \int_{\partial B_{se}} (\mathbf{Sn} - \bar{\mathbf{t}})\cdot\mathbf{u}\,\mathrm{d}S + \int_{\partial B_{ue}} \mathbf{Sn}\cdot\bar{\mathbf{u}}\,\mathrm{d}S \\ &+ \int_{\partial B_{de}} (\mathbf{d}\cdot\mathbf{n} + \bar{d})\,\phi\,\mathrm{d}S + \int_{\partial B_{\phi e}} \mathbf{d}\cdot\mathbf{n}\,\bar{\phi}\,\mathrm{d}S \Bigg] \\ &+ \sum_j \int_{\varrho_j} [(\mathbf{Sn})_j^+ + (\mathbf{Sn})_j^-]\cdot\mathbf{u}\,\mathrm{d}S + \sum_j \int_{\varrho_j} [(\mathbf{d}\cdot\mathbf{n})_j^+ + (\mathbf{d}\cdot\mathbf{n})_j^-]\phi\,\mathrm{d}S.\end{aligned} \tag{36}$$

With the same algebra used above, it is possible to realize that the stationary conditions of functional (36) are: the same stationary conditions of Eq. (22) for the typical subdomain, and the identification of functions $\mathbf{v}$ and $v$ with displacement $\mathbf{u}$ and electric potential $\phi$, respectively, for the typical interface, together with the transitional conditions on traction and electric flux

$$(\mathbf{Sn})_j^+ + (\mathbf{Sn})_j^- = \mathbf{0}, \quad (\mathbf{d}\cdot\mathbf{n})_j^+ + (\mathbf{d}\cdot\mathbf{n})_j^- = 0 \qquad \text{at } \varrho_j, \ \ j = 1, ..., m. \tag{37}$$

### 3.2. Hybrid stress formulation

The electric field $\mathbf{e}$ is eliminated between Eqs. (8) and (13) and the function

$$\psi_\phi(\mathbf{S},\phi) = -\tfrac{1}{2}\mathbf{H}^e\mathbf{S}\cdot\mathbf{S} - \tfrac{1}{2}\mathbf{k}^s\operatorname{grad}\phi\cdot\operatorname{grad}\phi + \mathbf{gS}\cdot\operatorname{grad}\phi \tag{38}$$

is obtained. Consider the functional

$$\Psi(\mathbf{S},\mathbf{u},\phi,d)=\int_B \psi_\phi(\mathbf{S},\phi)\,\mathrm{d}V+\int_B \gamma\,\phi\,\mathrm{d}V+\int_{\partial B_s}(\mathbf{S}\mathbf{n}-\bar{\mathbf{t}})\cdot\mathbf{u}\,\mathrm{d}S+\int_{\partial B_u}\mathbf{S}\mathbf{n}\cdot\bar{\mathbf{u}}\,\mathrm{d}S+\int_{\partial B_d}\bar{d}\,\phi\,\mathrm{d}S+\int_{\partial B_\phi} d(\phi-\bar{\phi})\mathrm{d}S, \tag{39}$$

jointly concave in $\mathbf{S}$ and $\mathbf{d}$, see Eq. (8). The domain of functional $\Psi$ is the cartesian product of the sets of functions $\mathbf{S}$ which satisfy equilibrium condition (16) and functions $\phi$ which satisfy compatibility condition (13), and of the sets of functions $\mathbf{u}$ and $d$ continuous on $\partial B_s$ and $\partial B_\phi$, respectively. The first variation of $\Psi$ reads as

$$\begin{aligned}\delta\Psi=&\int_B(-\mathbf{H}^e\mathbf{S}\cdot\delta\mathbf{S}+\mathbf{g}\,\delta\mathbf{S}\cdot\operatorname{grad}\phi-\mathbf{k}^s\operatorname{grad}\phi\cdot\operatorname{grad}\delta\phi+\mathbf{g}\mathbf{S}\cdot\operatorname{grad}\delta\phi)\mathrm{d}V+\int_B\gamma\,\delta\phi\,\mathrm{d}V\\&+\int_{\partial B_s}(\mathbf{S}\mathbf{n}-\bar{\mathbf{t}})\cdot\delta\mathbf{u}\,\mathrm{d}S+\int_{\partial B_s}\mathbf{u}\cdot\delta\mathbf{S}\mathbf{n}\,\mathrm{d}S+\int_{\partial B_u}\bar{\mathbf{u}}\cdot\delta\mathbf{S}\mathbf{n}\,\mathrm{d}S+\int_{\partial B_d}\bar{d}\,\delta\phi\,\mathrm{d}S+\int_{\partial B_\phi}\left(\phi-\bar{\phi}\right)\delta d\,\mathrm{d}S\\&+\int_{\partial B_\phi}d\,\delta\phi\,\mathrm{d}S,\end{aligned} \tag{40}$$

where the variation $\delta\mathbf{S}$ is subjected to the constraint $\operatorname{div}\delta\mathbf{S}=\mathbf{0}$. Let $\mathbf{v}$ denote a vector of functions of $\mathbf{x}$. The identically null term

$$-\int_B\operatorname{div}\delta\mathbf{S}\cdot\mathbf{v}\,\mathrm{d}V$$

is added to functional $\delta\Psi$, and applying identities (20) and (21) for sufficiently regular functions $\mathbf{S}$, $\mathbf{d}$, $\mathbf{u}$, $\phi$ and $\mathbf{v}$ leads to

$$\begin{aligned}\delta\Psi=&\int_B\{(\operatorname{symgrad}\mathbf{v}-\mathbf{H}^e\mathbf{S}+\mathbf{g}^{\mathrm{t}}\operatorname{grad}\phi)\cdot\delta\mathbf{S}+[\operatorname{div}(\mathbf{k}^s\operatorname{grad}\phi)-\mathbf{g}\mathbf{S}+\gamma]\delta\phi\}\mathrm{d}V\\&-\int_{\partial B_s}(\mathbf{v}-\mathbf{u})\cdot\delta\mathbf{S}\mathbf{n}\,\mathrm{d}S+\int_{\partial B_s}(\mathbf{S}\mathbf{n}-\bar{\mathbf{t}})\cdot\delta\mathbf{u}\,\mathrm{d}S-\int_{\partial B_u}\left(\mathbf{v}-\bar{\mathbf{u}}\right)\cdot\delta\mathbf{S}\mathbf{n}\,\mathrm{d}S\\&+\int_{\partial B_d}[\bar{d}-\mathbf{n}\cdot(\mathbf{g}\mathbf{S}+\mathbf{k}^s\operatorname{grad}\phi)]\delta\phi\,\mathrm{d}S+\int_{\partial B_\phi}[d-\mathbf{n}\cdot(\mathbf{g}\mathbf{S}+\mathbf{k}^s\operatorname{grad}\phi)]\delta\phi\,\mathrm{d}S-\int_{\partial B_\phi}(\phi-\bar{\phi})\delta d\,\mathrm{d}S.\end{aligned} \tag{41}$$

The variational equation

$$\delta\Psi=0\quad\forall(\delta\mathbf{S},\delta\mathbf{u},\delta\phi,\delta d) \tag{42}$$

yields the necessary and sufficient stationary conditions for functional $\Psi$ on the set of functions $\mathbf{S}$ fulfilling Eq. (16) and of functions $\phi$ differentiable in $B$:

$$\operatorname{symgrad}\mathbf{v}-\mathbf{H}^e\mathbf{S}+\mathbf{g}^{\mathrm{t}}\operatorname{grad}\phi=\mathbf{0}\quad\text{in } B, \tag{43}$$

$$\operatorname{div}(\mathbf{k}^s\operatorname{grad}\phi)-\mathbf{g}\mathbf{S}+\gamma=0\quad\text{in } B, \tag{44}$$

$$\mathbf{v}-\mathbf{u}=\mathbf{0}\quad\text{on } \partial B_s, \tag{45}$$

$$\mathbf{S}\mathbf{n}-\bar{\mathbf{t}}=\mathbf{0}\quad\text{on } \partial B_s, \tag{46}$$

$$\mathbf{v}-\bar{\mathbf{u}}=\mathbf{0}\quad\text{on } \partial B_u, \tag{47}$$

$$\mathbf{n}\cdot(\mathbf{g}\mathbf{S}+\mathbf{k}^s\operatorname{grad}\phi)-\bar{d}=0\quad\text{on } \partial B_d, \tag{48}$$

$$\phi-\bar{\phi}=0\quad\text{on } \partial B_\phi, \tag{49}$$

$$\mathbf{n}\cdot(\mathbf{g}\mathbf{S}+\mathbf{k}^s\operatorname{grad}\phi)-d=0\quad\text{on } \partial B_\phi. \tag{50}$$

It appears from Eqs. (43), (45) and (47) that if $\Psi$ is stationary there exists a vector $\mathbf{v}$ which identifies with displacement $\mathbf{u}$ so that the compatibility conditions (12) and (14) are fulfilled. In addition, boundary compatibility for $\phi$ and equilibrium conditions (17)–(19), with $\mathbf{d}$ expressed through Eqs. (10) and (13), are also fulfilled. Moreover, Eq. (50) defines the density of electric flux through $\partial B_\phi$. It follows that the stationary point of functional $\Psi$ corresponds to the solution of the electroelastic problem.

The requirements of regularity for functions $\mathbf{S}$ and $\phi$ can be relaxed on a finite number of interfaces in $B$ for finite element expansions, as in the previous case. With the notation of the previous Section, displacement $\mathbf{u}$ is assumed to be continuous on the typical interdomain, and electric potential $\phi$ is assumed to be differentiable on $B_e$ and continuous on the interdomain, whereas continuity of tractions through the interface between two contiguous subdomains, $(\mathbf{Sn})_j^+$ and $(\mathbf{Sn})_j^-$, is relaxed. Hence, functional (39) becomes

$$\Psi_D(\mathbf{S},\mathbf{d},\phi,d)=\sum_e\left[\int_{B_e}\psi_\phi(\mathbf{S},\phi)\,\mathrm{d}V+\int_{B_e}\gamma\,\phi\,\mathrm{d}V+\int_{\partial B_{se}}(\mathbf{Sn}-\bar{\mathbf{t}})\cdot\mathbf{u}\,\mathrm{d}S+\int_{\partial B_{ue}}\mathbf{Sn}\cdot\bar{\mathbf{u}}\,\mathrm{d}S\right.$$
$$\left.+\int_{\partial B_{de}}\bar{d}\,\phi\,\mathrm{d}S+\int_{\partial B_{\phi e}}d(\phi-\bar{\phi})\mathrm{d}S\right]+\sum_j\int_{\varrho_j}[(\mathbf{Sn})_j^+-(\mathbf{Sn})_j^-]\cdot\mathbf{u}\,\mathrm{d}S. \tag{51}$$

It is a matter of routine to realize that the stationary of functional (51) yields the same stationary conditions of functional (41) for the typical subdomain and the identification of function $\mathbf{v}$ with displacement $\mathbf{u}$ for the typical interface, together with the transitional conditions:

$$(\mathbf{Sn})_j^+-(\mathbf{Sn})_j^-=\mathbf{0},\quad\text{at }\varrho_j,\ \ j=1,\ldots,m. \tag{52}$$

## 4. Hybrid models and finite element implementation

Both the formulations presented above allow to implement a model and a finite element method of analysis. The model related to the first formulation is referred to as fully hybrid model, the one related to the second formulation as hybrid stress model.

### 4.1. Fully hybrid model

Functional (22) for the single element is written in the synthetic form

$$\Pi_e(\mathbf{S},\mathbf{d},\mathbf{u},\phi)=\int_{B_e}\pi(\mathbf{S},\mathbf{d})\,\mathrm{d}V+\int_{\partial B_e}(\mathbf{Sn}-\mathbf{t})\cdot\mathbf{u}\,\mathrm{d}S+\int_{\partial B_e}(\mathbf{d}\cdot\mathbf{n}+d)\,\phi\,\mathrm{d}S, \tag{53}$$

where $\mathbf{t}$ and $d$ are the traction and the electric flux density applied on $\partial B_e$, respectively. Note that if a part of $\partial B_e$ lies on $\partial B_s$ or $\partial B_d$, then $\mathbf{t}$ and $d$ should be specialized according to the prescribed conditions for forces or electric charges, respectively.

Both the stress and the electric flux density in each element are divided into two parts. The first part of each field is a particular solution of the relevant equilibrium equation, while the second part is required to satisfy the relevant equilibrium equation in the homogeneous form. This is written as

$$\mathbf{S}=\mathbf{S}_p+\mathbf{S}_0, \tag{54a}$$

$$\mathbf{d}=\mathbf{d}_p+\mathbf{d}_0, \tag{54b}$$

where

$$\operatorname{div}\mathbf{S}_p = -\mathbf{b}, \tag{55a}$$
$$\operatorname{div}\mathbf{S}_0 = \mathbf{0}, \tag{55b}$$

$$\operatorname{div}\mathbf{d}_p = \gamma, \tag{56a}$$
$$\operatorname{div}\mathbf{d}_0 = 0. \tag{56b}$$

The standard matrix–vector notation (Voigt, 1910) is employed for the subsequent expansions and the previous relations are intended as adjusted in accordance. The two parts of stress and electric flux density are expressed as

$$\mathbf{S}_0 = \mathbf{P}_s\beta_s, \quad \mathbf{S}_p = \bar{\mathbf{P}}_s\bar{\beta}_s, \tag{57}$$
$$\mathbf{d}_0 = \mathbf{P}_d\beta_d, \quad \mathbf{d}_p = \bar{\mathbf{P}}_d\bar{\beta}_d, \tag{58}$$

where vectors $\mathbf{S}_0 = \{\sigma^0_{ij}\}$ and $\mathbf{S}_p = \{\sigma^p_{ij}\}$ collect the independent stress tensor components, $\mathbf{P}_s$ and $\mathbf{P}_d$ are matrices of basis functions of $\mathbf{x}$ (i.e. of stress and electric flux modes), $\beta_s$ and $\beta_d$ are the vectors of unknown stress and electric flux parameters, matrices $\bar{\mathbf{P}}_s$ and $\bar{\mathbf{P}}_d$ are load and electric charge modes, functions of $\mathbf{x}$, and $\bar{\beta}_s$ and $\bar{\beta}_d$ are vectors of known coefficients. The null-divergence stress and electric flux density states, $\mathbf{S}_0$ and $\mathbf{d}_0$, can be built up starting from six algebraic functions of $\mathbf{x}$, say $\Phi^S_i = \Phi^S_i(\mathbf{x})$ and $\Phi^d_i = \Phi^d_i(\mathbf{x})$, $i = 1, 2, 3$ – stress and stream functions, respectively. Here they are obtained in accordance with the following scheme:

$$\sigma^0_{11} = \Phi^S_{1/2,3}, \quad \sigma^0_{22} = \Phi^S_{2/1,3}, \quad \sigma^0_{33} = \Phi^S_{3/1,2}, \tag{59}$$
$$\sigma^0_{12} = \Phi^S_{3/3,3}, \quad \sigma^0_{13} = \Phi^S_{2/2,2}, \quad \sigma^0_{23} = \Phi^S_{1/1,1}, \tag{60}$$
$$d^0_1 = \Phi^d_{1/2,3}, \quad d^0_2 = \Phi^d_{2/1,3}, \quad d^0_3 = \Phi^d_{3/1,2}, \tag{61}$$

under the constraints

$$\Phi^S_{1/1} + \Phi^S_{2/2} + \Phi^S_{3/3} = 0, \tag{62a}$$
$$\Phi^d_1 + \Phi^d_2 + \Phi^d_3 = 0, \tag{62b}$$

where the symbol $_{/i}$ denotes differentiation with respect to $x_i$. It is easy to verify that both the above sets of assumptions fulfill conditions (55b) and (56b), respectively. The stress function scheme adopted is due to Zanaboni (1936).

The displacement and the electric potential along the element boundary $\partial B_e$ are interpolated in terms of nodal amplitudes $\mathbf{q}_u$ and $\mathbf{q}_\phi$, respectively, in the form

$$\mathbf{u} = \mathbf{L}_u\mathbf{q}_u, \tag{63a}$$
$$\phi = \mathbf{L}_\phi\mathbf{q}_\phi, \tag{63b}$$

where $\mathbf{L}_u$ and $\mathbf{L}_\phi$ are matrices of shape functions.

The stationary conditions of the function which results from substituting the above assumptions into Eq. (53) yield the (mechanical and electrical) compatibility equations and the (force and electric charge) equilibrium equations of the model. These equations can be written in a compact form as

$$\begin{vmatrix} \mathbf{0} \\ \mathbf{0} \\ \mathbf{h}_u \\ \mathbf{h}_\phi \end{vmatrix} = \begin{vmatrix} -\mathbf{H}_s & -\mathbf{H}_{sd} & \mathbf{G}^{\mathrm{t}}_s & \mathbf{0} \\ -\mathbf{H}^{\mathrm{t}}_{sd} & \mathbf{H}_d & \mathbf{0} & \mathbf{G}^{\mathrm{t}}_d \\ \mathbf{G}_s & \mathbf{0} & \mathbf{0} & \mathbf{0} \\ \mathbf{0} & -\mathbf{G}_d & \mathbf{0} & \mathbf{0} \end{vmatrix} \begin{vmatrix} \beta_s \\ \beta_d \\ \mathbf{q}_u \\ \mathbf{q}_\phi \end{vmatrix} + \begin{vmatrix} \mathbf{g}_s \\ \mathbf{g}_d \\ \mathbf{g}_u \\ \mathbf{g}_\phi \end{vmatrix}, \tag{64}$$

where the expressions of all the matrices and vectors involved are given in Appendix A (I). Vectors $\mathbf{h}_u$ and $\mathbf{h}_\phi$ are, by definition, the generalized nodal forces and nodal electric charges, respectively. Matrices $\mathbf{H}_s$ and

$\mathbf{H}_d$ are symmetric and positive definite, and represent the elastic and electric compliance matrices of the model, matrix $\mathbf{H}_{sd}$ accounts for the electroelastic coupling, and matrices $\mathbf{G}_s$ and $\mathbf{G}_d$ are the mechanical and electrical load connection matrices, respectively. Vectors $\mathbf{g}_s$, $\mathbf{g}_d$, $\mathbf{g}_u$ and $\mathbf{g}_\phi$ collect known nodal values resulting from the mechanical and electrical quantities prescribed over the element domain.

Solving the compatibility equations in terms of the inner parameters $\beta_s$ and $\beta_d$ and substituting back into Eq. (64) leads to the coupled relation between nodal forces/charges and nodal displacements/potentials:

$$\left|\begin{array}{c}\mathbf{h}_u\\ \mathbf{h}_\phi\end{array}\right| = \left|\begin{array}{cc}\mathbf{K}_u & \mathbf{K}_{u\phi}^{\mathrm{t}}\\ -\mathbf{K}_{u\phi} & \mathbf{K}_\phi\end{array}\right|\left|\begin{array}{c}\mathbf{q}_u\\ \mathbf{q}_\phi\end{array}\right| + \left|\begin{array}{c}\mathbf{f}_u\\ \mathbf{f}_\phi\end{array}\right|, \tag{65}$$

where $\mathbf{K}_u$ is the stiffness matrix, $\mathbf{K}_\phi$ is the dielectric matrix, and $\mathbf{K}_{u\phi}$ is the electroelastic coupling matrix of the model. Vectors $\mathbf{f}_u$ and $\mathbf{f}_\phi$ collect the equivalent nodal forces and electric charges. Matrices $\mathbf{K}_u$ and $\mathbf{K}_\phi$ are symmetric and positive semidefinite. All the matrices and vectors in Eq. (65) are defined in Appendix A (II).

The approximate solution of the discrete electroelastic problem is obtained by solving the linear algebraic system of equations which results from assembling Eq. (65) for all the elements and thereafter enforcing the boundary conditions on displacements and electric potential (Zienkiewicz and Taylor, 1989).

### 4.2. Hybrid stress model

Functional (38) for the typical element can be cast in the compact form

$$\Psi_e(\mathbf{S},\mathbf{u},\phi) = \int_{B_e}\psi_\phi(\mathbf{S},\phi)\,\mathrm{d}V + \int_{B_e}\gamma\,\phi\,\mathrm{d}V + \int_{\partial B_e}(\mathbf{S}\mathbf{n}-\mathbf{t})\cdot\mathbf{u}\,\mathrm{d}S + \int_{\partial B_e} d\,\phi\,\mathrm{d}S, \tag{66}$$

where traction $\mathbf{t}$ and electric flux density $d$ should be specialized according to the prescribed boundary conditions if $\partial B_e$ lies on $\partial B_s$ or $\partial B_d$.

As regards the assumptions on the mechanical variables, the guidelines outlined for the fully hybrid model still hold. In particular, the stress field is split into two parts according to Eqs. (54a) and (55a,b), and the null-divergence part is obtained from three algebraic stress functions $\Phi_i^S = \Phi_i^S(\mathbf{x})$, $i = 1,2,3$, via Eqs. (59), (60) and (62a). The interelement displacement is interpolated on $\partial B_e$ by means of shape functions and nodal amplitudes as indicated by Eq. (63a).

Unlike the previous model, the electric potential is defined over the element domain and is interpolated in terms of nodal values as usual for the compatible approach (Allik and Hughes, 1970). In particular, it is represented in the form of Eq. (63b), where the shape functions are defined on $B_e$.

The stationary of the function which results from substituting the above assumptions into Eq. (66) leads to the mechanical compatibility equation and to the force and electric charge equilibrium equations of the model. These equations can be cast in the compact form

$$\left|\begin{array}{c}\mathbf{0}\\ \mathbf{h}_u\\ \mathbf{h}_\phi\end{array}\right| = \left|\begin{array}{ccc}-\mathbf{H}_s & \mathbf{G}_s^{\mathrm{t}} & \mathbf{W}_{s\phi}^{\mathrm{t}}\\ \mathbf{G}_s & \mathbf{0} & \mathbf{0}\\ -\mathbf{W}_{s\phi} & \mathbf{0} & \mathbf{W}_\phi\end{array}\right|\left|\begin{array}{c}\beta_s\\ \mathbf{q}_u\\ \mathbf{q}_\phi\end{array}\right| + \left|\begin{array}{c}\mathbf{g}_s\\ \mathbf{g}_u\\ \mathbf{g}_\phi\end{array}\right|, \tag{67}$$

where vectors $\mathbf{h}_u$ and $\mathbf{h}_\phi$ are (the definition of) the generalized nodal forces and nodal electric charges, respectively, matrix $\mathbf{W}_{s\phi}$ accounts for the electroelastic coupling, and the known vectors $\mathbf{g}_s$, $\mathbf{g}_u$ and $\mathbf{g}_\phi$ account for the mechanical and electrical quantities prescribed over the element domain. Matrix $\mathbf{H}_s$ and $\mathbf{W}_\phi$ are symmetric and positive definite. All the matrices and vectors involved in Eq. (67) are defined in Appendix B (I).

Eliminating the stress parameters $\beta_s$ through the mechanical compatibility equation yields a system of coupled equations formally analogous to Eq. (65). The expressions of the matrices and vectors involved are

defined in Appendix B (II). Assembling all the elements and enforcing the boundary conditions on displacements and electric potential are accomplished following the standard finite element procedure.

### 4.3. Implementation

The finite element implementation of the above models requires some considerations about stability and invariance.

Stability is met if no spurious or zero energy modes arise, that is if both the stiffness and dielectric matrices are rank sufficient (e.g. Brezzi and Fortin, 1991). For the fully hybrid model, the necessary conditions for stability are

$$n_s \geqslant n_u - 6, \tag{68a}$$

$$n_d \geqslant n_\phi - 1, \tag{68b}$$

where $n_s$, $n_u$, $n_d$ and $n_\phi$ are the number of parameters in the representation assumed for $\mathbf{S}$, $\mathbf{u}$, $\mathbf{d}$ and $\phi$, respectively, 6 is the number of the element rigid body degrees of freedom, and 1 stands for the constant electric potential distribution which is admitted with zero electric field. For the hybrid stress model, the stability requirement reduces only to the condition (68a).

The above conditions state the minimum number of parameters, i.e. of stress and electric flux independent modes for an assumed representation of displacement and electric potential. It is worthwhile to underline that the number of the introduced modes should be as close as possible to the minimum. In fact, the smaller the number of modes the lower is the computing cost for eliminating the relevant parameters at the element level. Moreover, a large number of stress modes could lead to increased stiffness (Pian, 1973), and analogous effect could occur for electric flux density.

An element should be invariant with respect to any coordinate change, so that the implementation is independent of the reference coordinate frame adopted (Sze et al., 1992). This requirement is met if the representations assumed for $\mathbf{S}$ and $\mathbf{d}$ (or only for $\mathbf{S}$ in the case of the hybrid stress model) are complete. In fact, a complete polynomial basis does not change under a linear transformation of coordinates, i.e. by changing the reference system. In the present context, invariance is met if complete functions $\Phi_i^S$ and $\Phi_i^d$ are assumed. Otherwise, invariance is retained only for the modes up to the maximum degree of completeness.

As regards the computational effort, both the hybrid models require the elimination of the inner parameters at the element level. Stress and electric flux parameters are to be eliminated in the fully hybrid model, whereas only stress parameters are eliminated in the hybrid stress one. However, the higher computational burden involved with respect to the standard displacement-potential finite element approach is generally offset by the higher accuracy in the results, as the following numerical tests show.

## 5. Numerical tests

Four hexahedral isoparametric finite elements have been implemented following the guidelines exposed in the previous section. Two elements, indicated by FH8 and FH20, are of fully hybrid type, and the other two, indicated by HS8 and HS20, are of hybrid stress type. Element FH8 is based on the eight-node scheme (vertex nodes), where displacement and electric potential are represented on each face by bilinear shape functions. The stress and the electric flux representations are obtained from complete quartic functions $\Phi_i^S$ and $\Phi_i^d$. Element FH20 is based on the twenty-node scheme (vertex and midedge nodes), where displacement and electric potential are represented on each face by quadratic serendipity shape functions. The stress and the electric flux representations are obtained from complete quintic functions $\Phi_i^S$ and $\Phi_i^d$. The two hybrid stress elements HS8 and HS20 have stress and displacement represented as in FH8 and FH20,

Table 1
Elastic, electroelastic and dielectric moduli of ceramic PZT-5H

| $C_{11}$ (GPa) | $C_{33}$ (GPa) | $C_{12}$ (GPa) | $C_{13}$ (GPa) | $C_{44}$ (GPa) | $c_{31}$ (C/m$^2$) | $c_{33}$ (C/m$^2$) | $c_{15}$ (C/m$^2$) | $k_{11}$ (nF/m) | $k_{33}$ (nF/m) |
|---|---|---|---|---|---|---|---|---|---|
| 126.0 | 117.0 | 79.5 | 84.1 | 23.0 | −6.5 | 23.3 | 17.0 | 15.0 | 13.0 |

respectively. The electric potential is interpolated by standard trilinear shape functions for HS8 (eight-node scheme) and by triquadratic serendipity shape functions for HS20 (20-node scheme).

The performance of the above elements is compared with the one of standard, compatible eight-node and 20-node hexahedral isoparametric elements, based on electric enthalpy as energy function, Eq. (1), i.e. having displacement and electric potential as variables. The compatible elements are denoted by C8 and C20, respectively. The Gaussian quadrature rule is used for both hybrid and compatible elements. In the fully hybrid elements the integrals are evaluated exactly, while in the hybrid stress and compatible elements the proper number of quadrature points for the exact integration in regular geometry is employed.

Reference is made to a transversely isotropic homogeneous square plate of edge $L$ and thickness $H$, made of piezoelectric ceramic PZT-5H (Bisegna and Maceri, 1996). The transverse isotropy axis is orthogonal to the midsurface of the plate. On the lateral faces of the plate, the tangential component of the displacement and the electric potential are assumed to vanish. The values of the material constants (at room temperature) are collected in Table 1, where $C_{ij}$, $c_{ij}$ and $k_{ij}$ are, in matrix notation, the coefficients of the elastic, electroelastic and dielectric tensors, respectively.

Two different load cases are considered: a uniform normal surface force of intensity $q/2$ both on the upper and on the lower face (Fig. 1(a)) and a uniform surface electric charge of density $\omega$ on the upper face and of density $-\omega$ on the lower face (Fig. 1(b)). The plate shows a flexural behavior in the first case, and an in-plane behavior in the second one. Both the cases are solved by uniformly increasing the in-plane discretization. Two and four eight-node elements, and one and two 20-node elements are used in the thickness direction. The finite element solutions are compared with the results obtained from the three-dimensional solution presented by Bisegna and Maceri (1996).

The relative percent errors in displacement $u_3$ and electric potential $\phi$, both of them evaluated at the center of the plate, are plotted against the number of in-plane elements in Figs. 2 and 3, and the related values are listed in Tables 2 and 3. Figures and tables refer to the first and the second load case, respectively, and are obtained for the value $H/L = 1/5$ of the thickness-to-side ratio of the plate. The number of elements in $x_1$-, $x_2$- and $x_3$-direction are denoted by $n_1$, $n_2$ and $n_3$, respectively.

The graphs show that the fully hybrid elements globally perform better than the hybrid stress elements and the compatible ones with the same number of nodes. In fact, the error values in both displacement and

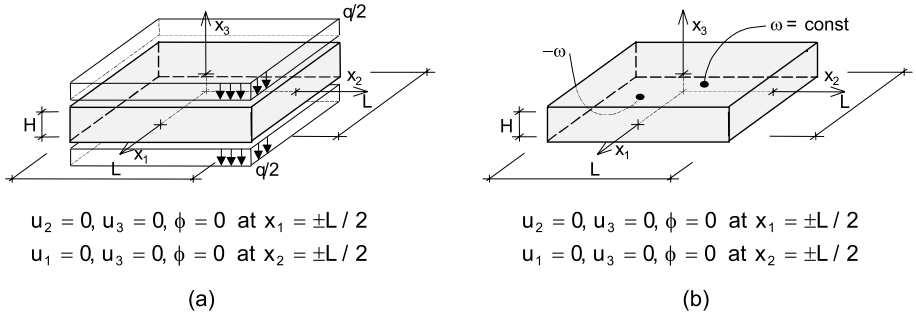


Fig. 1. Square plate in PZT-5H ceramic.

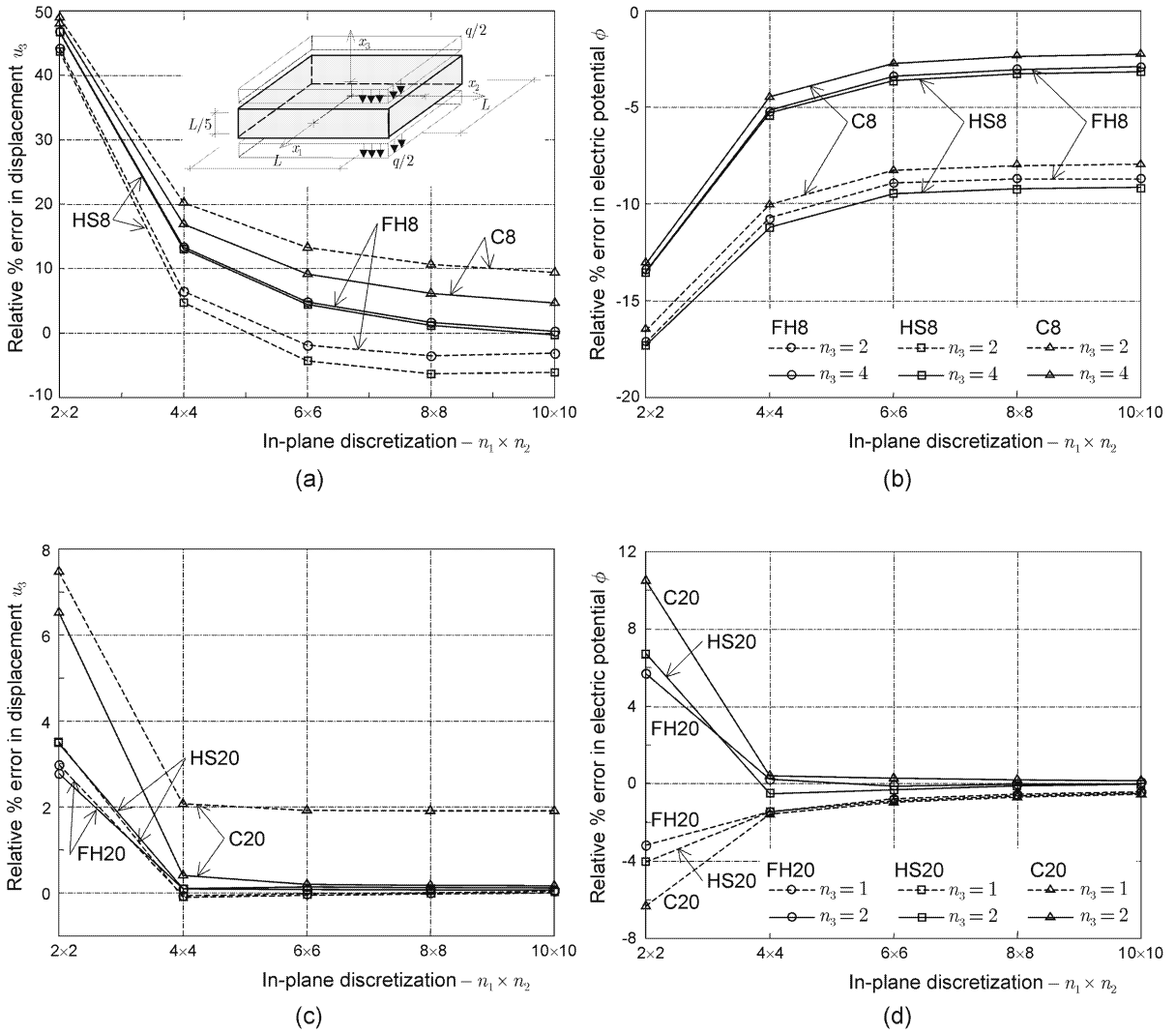


Fig. 2. Case 1, $H/L = 1/5$: convergence tests in the center of the plate. Relative percent errors in: (a) displacement $u_3$ and (b) electric potential $\phi$ for eight-node elements, (c) displacement $u_3$ and (d) electric potential $\phi$ for 20-node elements.

electric potential which result from the fully hybrid elements are the smallest for both the load cases. The hybrid stress elements exhibit an intermediate performance between the compatible and fully hybrid ones. Indeed, the error values resulting from the hybrid stress elements are closer to those of the fully hybrid elements rather than to those of the compatible ones.

The results obtained using 20-node elements and a $4 \times 4 \times 2$ element mesh are presented in detail for the thick plate with thickness-to-side ratio equal to $2/5$. In the case of surface forces prescribed, Fig. 4 shows the normalized transversal displacement $\hat{u}_3$, electric potential $\hat{\phi}$, in-plane normal stress $\hat{\sigma}_{11}$ and in-plane electric flux density $\hat{d}_1$ in the thickness direction. In the case of surface electric charge prescribed, Fig. 5 shows the normalized in-plane displacement $\hat{u}_1$, electric potential $\hat{\phi}$, in-plane normal stress $\hat{\sigma}_{11}$ and transversal electric flux density $\hat{d}_3$ in the thickness direction. The definitions of the dimensionless quantities plotted in both the

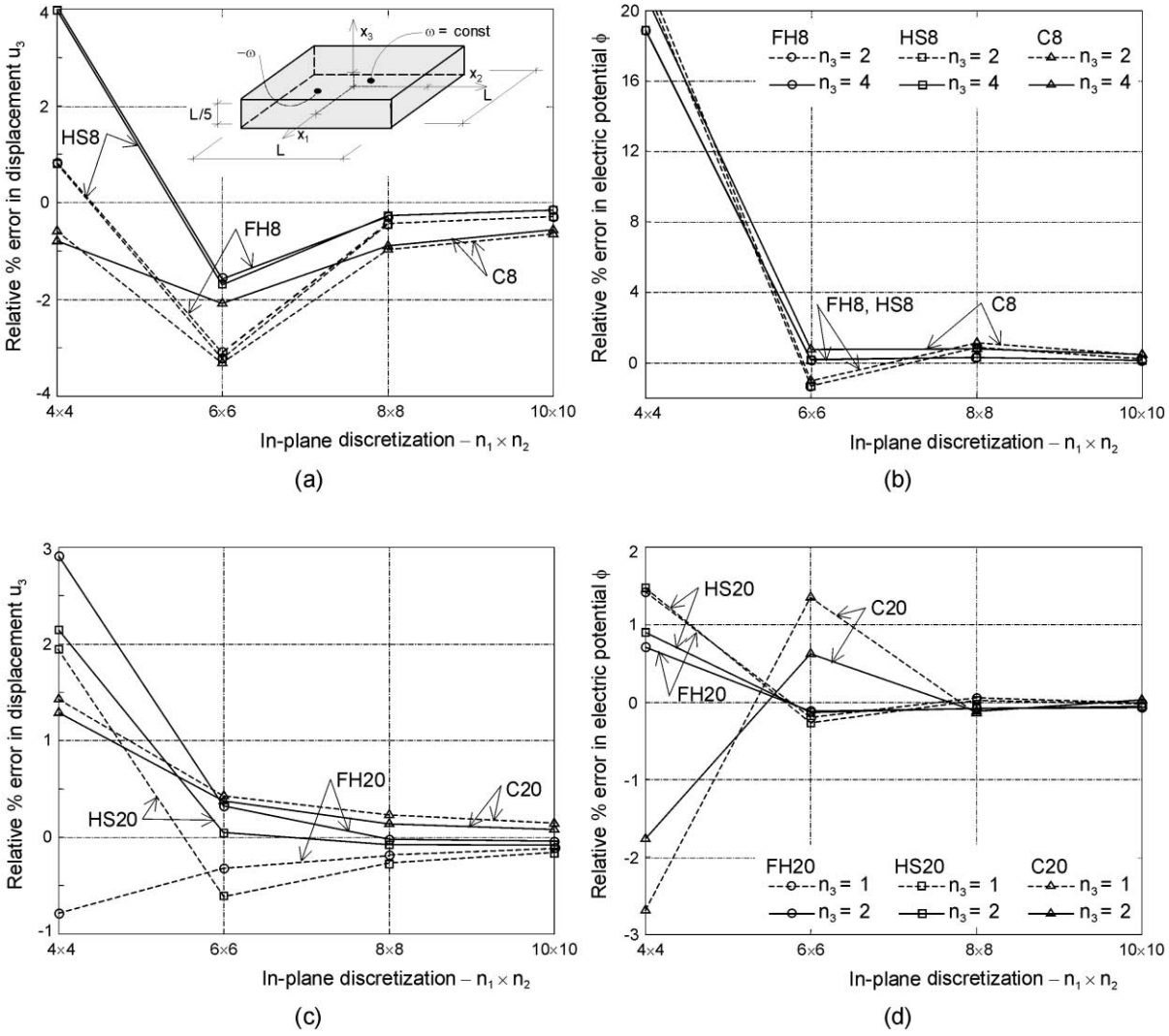


Fig. 3. Case 2, $H/L = 1/5$: convergence tests in the center of the bottom surface. Relative percent errors in: (a) displacement $u_3$ and (b) electric potential $\phi$ for eight-node elements, (c) displacement $u_3$ and (d) electric potential $\phi$ for 20-node elements.

figures are given in Appendix C. The graphs of normal stress and electric flux result from connecting with straight lines the values obtained in five Gauss points and two boundary points for each element crossed by the section line.

Inspecting the figures reveals the highest accuracy of the fully hybrid model in predicting both the mechanical and the electrical quantities. In particular, notice that also the stress and the electric flux distributions are in good agreement with the reference solution for both the load cases (Fig. 4(c), (d) and Fig. 5(c), (d)). As regards the hybrid stress model, it appears to be globally more accurate than the compatible one. In the case of the plate subjected to surface forces, the predictions of the hybrid stress element are comparable with those of the fully hybrid one, even though slightly less accurate (Fig. 4). Notice that the hybrid stress element shows near continuity of the normal stress across the interelement boundary

Table 2
Case 1, $H/L = 1/5$: relative percent error in the central deflection and electric potential

| Element | | | Number of in-plane elements – $n_1 \times n_2$ | | | | |
|---|---|---|---|---|---|---|---|
| | | | $2 \times 2$ | $4 \times 4$ | $6 \times 6$ | $8 \times 8$ | $10 \times 10$ |
| FH8 | $n_3 = 2$ | $\hat{u}_3$ | 44.182 | 6.433 | −1.909 | −3.576 | −3.170 |
| | | $\hat{\phi}$ | −17.066 | −10.469 | −8.756 | −8.554 | −8.410 |
| | $n_3 = 4$ | $\hat{u}_3$ | 46.831 | 13.331 | 4.806 | 1.638 | 0.237 |
| | | $\hat{\phi}$ | −13.403 | −5.105 | −3.372 | −3.034 | −2.894 |
| FH20 | $n_3 = 1$ | $\hat{u}_3$ | 2.974 | −0.069 | −0.024 | 0.006 | 0.031 |
| | | $\hat{\phi}$ | −3.182 | −1.464 | −0.786 | −0.556 | −0.423 |
| | $n_3 = 2$ | $\hat{u}_3$ | 2.839 | 0.125 | 0.142 | 0.133 | 0.125 |
| | | $\hat{\phi}$ | 5.702 | 0.229 | −0.129 | 0.007 | 0.071 |
| HS8 | $n_3 = 2$ | $\hat{u}_3$ | 43.745 | 4.752 | −4.314 | −6.388 | −6.149 |
| | | $\hat{\phi}$ | −17.163 | −10.817 | −9.225 | −8.849 | −8.656 |
| | $n_3 = 4$ | $\hat{u}_3$ | 46.740 | 13.030 | 4.404 | 1.168 | −0.291 |
| | | $\hat{\phi}$ | −13.432 | −5.190 | −3.479 | −3.156 | −3.030 |
| HS20 | $n_3 = 1$ | $\hat{u}_3$ | 3.330 | −0.085 | −0.042 | −0.008 | 0.021 |
| | | $\hat{\phi}$ | −4.061 | −1.470 | −0.883 | −0.646 | −0.516 |
| | $n_3 = 2$ | $\hat{u}_3$ | 3.305 | 0.120 | 0.155 | 0.142 | 0.133 |
| | | $\hat{\phi}$ | 6.730 | −0.540 | −0.336 | −0.126 | −0.042 |
| C8 | $n_3 = 2$ | $\hat{u}_3$ | 48.959 | 20.239 | 13.292 | 10.639 | 9.369 |
| | | $\hat{\phi}$ | −16.542 | −10.033 | −8.278 | −8.035 | −7.923 |
| | $n_3 = 4$ | $\hat{u}_3$ | 48.029 | 16.930 | 9.114 | 6.112 | 4.663 |
| | | $\hat{\phi}$ | −13.120 | −4.450 | −2.752 | −2.392 | −2.257 |
| C20 | $n_3 = 1$ | $\hat{u}_3$ | 7.478 | 2.075 | 1.923 | 1.905 | 1.905 |
| | | $\hat{\phi}$ | −6.349 | −1.582 | −0.969 | −0.721 | −0.562 |
| | $n_3 = 2$ | $\hat{u}_3$ | 6.520 | 0.404 | 0.203 | 0.172 | 0.162 |
| | | $\hat{\phi}$ | 10.499 | 0.398 | 0.265 | 0.190 | 0.145 |

(Fig. 4(c)) as well as the fully hybrid one. In the case of the plate subjected to the surface electric charges, the displacement and electric potential predictions of the hybrid stress element are comparable with those of the compatible one, even though slightly more accurate (Fig. 5(a) and (b)). On the other hand, a higher accuracy is obtained in determining the stress distribution (Fig. 5(c)). Finally, both the hybrid stress and the compatible elements show an apparently anomalous behavior in predicting the electric flux distribution (Fig. 5(d)). This fact depends on the relative coarseness of the $4 \times 4 \times 2$ mesh, as well as the poor accuracy of C20 in the stress recovery (Fig. 5(c)). Indeed, using a mesh of four elements in the thickness and six by six elements in the plane leads to a qualitative behavior less far from the one of the reference solution, but yet less accurate than the one of FH20 (Fig. 5(d)). The better qualitative results of the fully hybrid model in predicting the stress and the electric flux density can be interpreted based on the fact that both these variables are directly represented in the model. The same holds for the hybrid stress model with regard to stresses.

The behavior of the hybrid models has been investigated also for other values of the thickness-to-side ratio of the plate (Cannarozzi and Ubertini, 1999). In order to account for the performance of the hybrid models for thin plates, it seems sufficient to present the results obtained for the value $H/L = 1/10$ of the thickness-to-side ratio of the plate in Figs. 6 and 7. These results appear slightly less accurate than the ones for $H/L = 2/5$. Indeed, this is due to the fact that the same mesh is used for both the thickness-to-side ratios, so that the element aspect ratio for $H/L = 1/10$ turns out to be quite severe. This provided, the better behavior of the hybrid models in comparison with the compatible model experienced for all the cases above is confirmed.

Table 3
Case 2, $H/L = 1/5$: relative percent error in the deflection and electric potential at the center of the bottom face

| Element | | | Number of in-plane elements – $n_1 \times n_2$ | | | |
|---|---|---|---|---|---|---|
| | | | $4 \times 4$ | $6 \times 6$ | $8 \times 8$ | $10 \times 10$ |
| FH8 | $n_3 = 2$ | $\hat{u}_3$ | 0.825 | −3.002 | −0.308 | −0.288 |
| | | $\hat{\phi}$ | 21.334 | −1.301 | 0.845 | 0.201 |
| | $n_3 = 4$ | $\hat{u}_3$ | 4.056 | −1.634 | −0.259 | −0.157 |
| | | $\hat{\phi}$ | 18.807 | 0.165 | 0.291 | 0.135 |
| FH20 | $n_3 = 1$ | $\hat{u}_3$ | −0.790 | −0.451 | −0.360 | −0.156 |
| | | $\hat{\phi}$ | 1.423 | −0.197 | 0.055 | −0.039 |
| | $n_3 = 2$ | $\hat{u}_3$ | 2.911 | 0.325 | −0.038 | −0.078 |
| | | $\hat{\phi}$ | 0.716 | −0.114 | −0.079 | −0.027 |
| HS8 | $n_3 = 2$ | $\hat{u}_3$ | 0.808 | −3.125 | −0.310 | −0.290 |
| | | $\hat{\phi}$ | 21.427 | −1.323 | 0.865 | 0.208 |
| | $n_3 = 4$ | $\hat{u}_3$ | 3.982 | −1.712 | −0.269 | −0.160 |
| | | $\hat{\phi}$ | 18.882 | 0.167 | 0.292 | 0.138 |
| HS20 | $n_3 = 1$ | $\hat{u}_3$ | 1.946 | −0.675 | −0.392 | −0.222 |
| | | $\hat{\phi}$ | 1.487 | −0.252 | 0.107 | −0.041 |
| | $n_3 = 2$ | $\hat{u}_3$ | 2.149 | 0.065 | −0.126 | −0.134 |
| | | $\hat{\phi}$ | 0.965 | −0.123 | −0.086 | −0.029 |
| C8 | $n_3 = 2$ | $\hat{u}_3$ | −0.593 | −3.313 | −0.976 | −0.654 |
| | | $\hat{\phi}$ | 22.027 | −1.044 | 1.120 | 0.484 |
| | $n_3 = 4$ | $\hat{u}_3$ | −0.795 | −2.084 | −0.904 | −0.569 |
| | | $\hat{\phi}$ | 20.873 | 0.757 | 0.777 | 0.474 |
| C20 | $n_3 = 1$ | $\hat{u}_3$ | 1.430 | 0.425 | 0.319 | 0.223 |
| | | $\hat{\phi}$ | −2.604 | 1.340 | −0.177 | 0.054 |
| | $n_3 = 2$ | $\hat{u}_3$ | 1.288 | 0.395 | 0.265 | 0.151 |
| | | $\hat{\phi}$ | −1.779 | 0.668 | −1.121 | 0.032 |

The sensitivity of the hybrid models to element geometry distortions is investigated for $H/L = 2/5$ by solving both the two load cases using different meshes with progressively distorted elements (Fig. 8). The distortion is measured by the parameter $d/L$, which ranges from 0 to 0.375. For brevity, a comparison among 20-node elements only has been included, but the conclusions which are drawn hold for eight-node elements also. The normalized displacement $\hat{u}_3$ and the normalized electric potential $\hat{\phi}$ are plotted versus the distortion parameter in Fig. 9. The plotted quantities are evaluated at the center of the plate for the first load case (Fig. 9(a) and (b)), and at the center of the lower face for the second load case (Fig. 9(c) and (d)).

As it can be observed, the fully hybrid element appears to be much less sensitive to element geometry distortions than the compatible and the hybrid stress one. On this regard, notice that the hybrid stress element seems to be globally less sensitive than the compatible one.

## 6. Concluding remarks

The two methods presented for the linear electroelastic analysis are alternative to the standard compatible approach, based on displacement and electric potential interpolation. In the outlined variational framework, two finite element models are developed and a comprehensive guideline for their implementation is presented. Both the models perform better than the standard, compatible finite element model, as shown in the numerical tests presented. The fully hybrid model appears to be the most accurate in

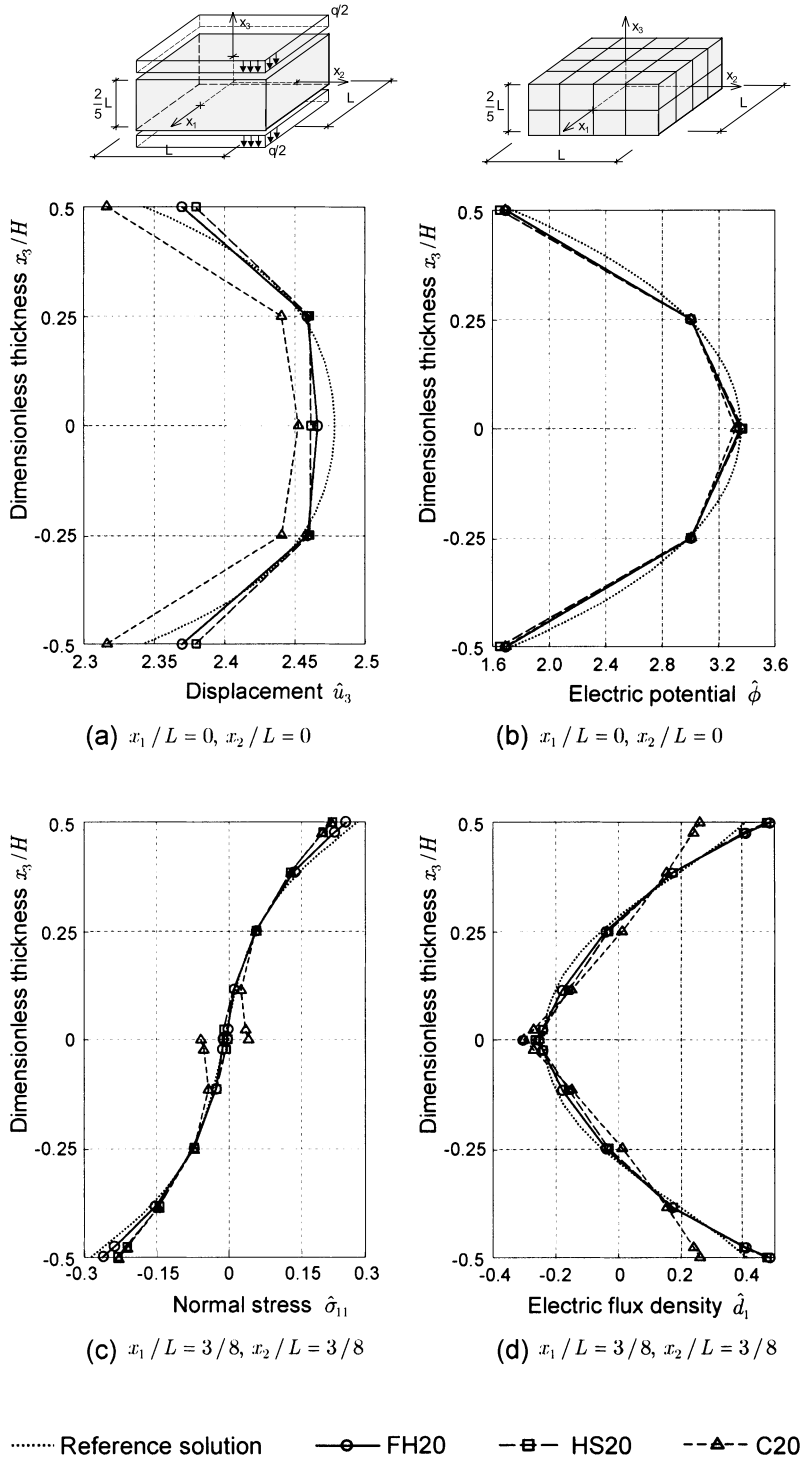


Fig. 4. Case 1, $H/L = 2/5$: (a) normalized displacement $\hat{u}_3$, (b) normalized electric potential $\hat{\phi}$, (c) normalized normal stress $\hat{\sigma}_{11}$ and (d) normalized electric flux density $\hat{d}_1$ in the thickness direction.

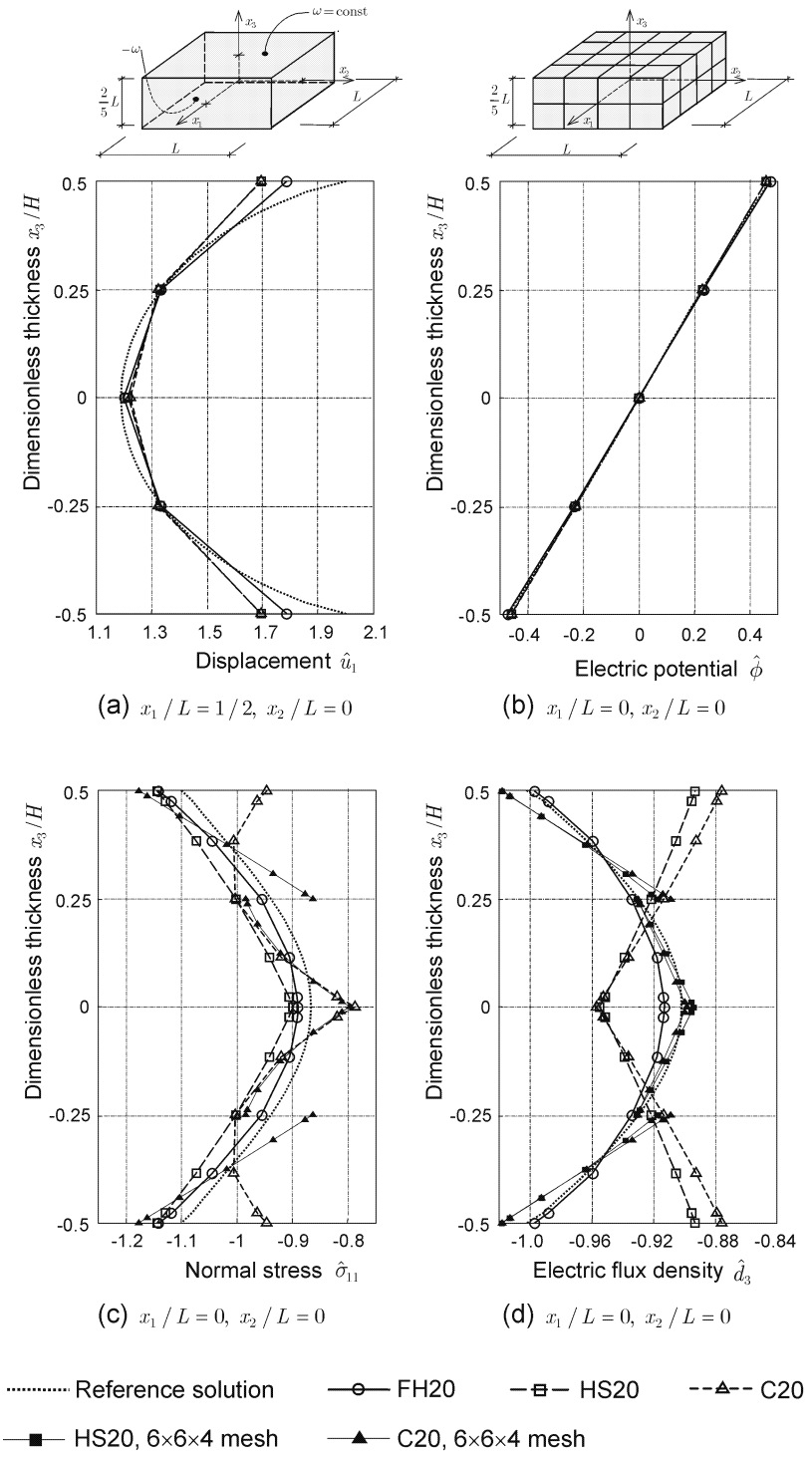


Fig. 5. Case 2, $H/L = 2/5$: (a) normalized displacement $\hat{u}_1$, (b) normalized electric potential $\hat{\phi}$, (c) normalized normal stress $\hat{\sigma}_{11}$ and (d) normalized electric flux density $\hat{d}_3$ in the thickness direction.

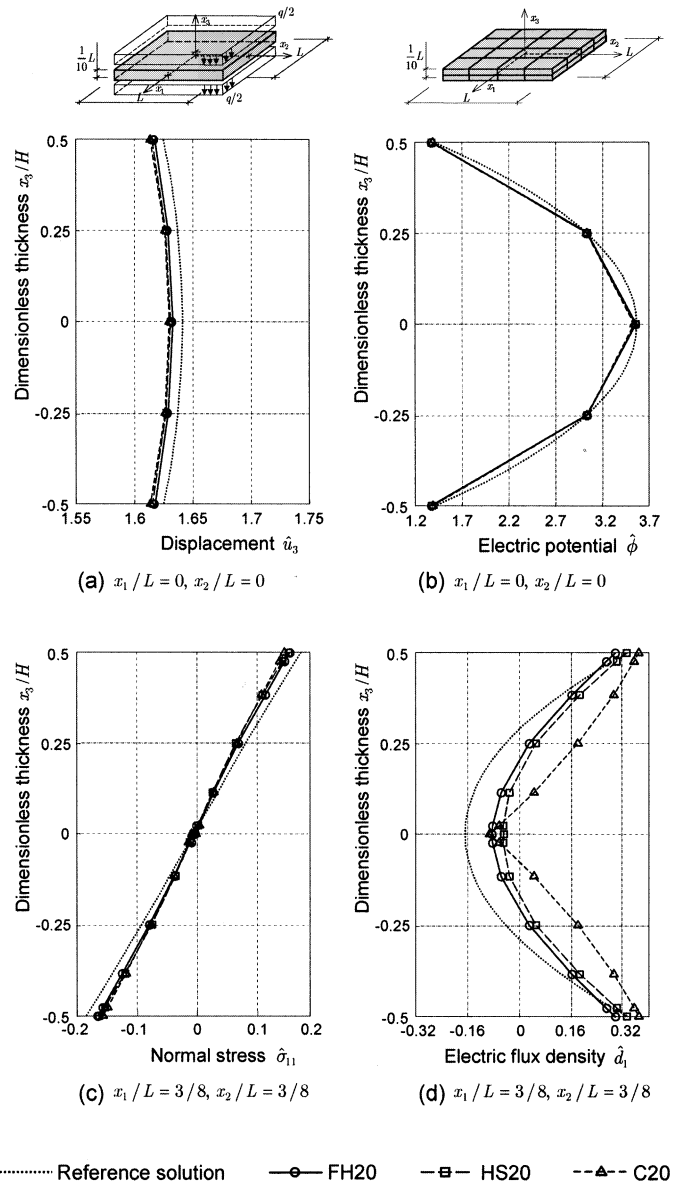


Fig. 6. Case 1, $H/L = 1/10$: (a) normalized displacement $\hat{u}_3$, (b) normalized electric potential $\hat{\phi}$, (c) normalized normal stress $\hat{\sigma}_{11}$ and (d) normalized electric flux density $\hat{d}_1$ in the thickness direction.

predicting either displacement and stress or electric potential and flux density, and only slightly sensitive to element geometry distortions. Thus, it seems the most reliable for electroelastic analysis. The hybrid stress model shows an intermediate behavior between the fully hybrid and the compatible one. In particular, its accuracy is generally comparable with the fully hybrid model in predicting the mechanical variables and with the compatible model in predicting the electrical ones. Thus, it appears more effective than the compatible approach and generally reliable for electroelastic analysis when the mechanical part is of primary importance.

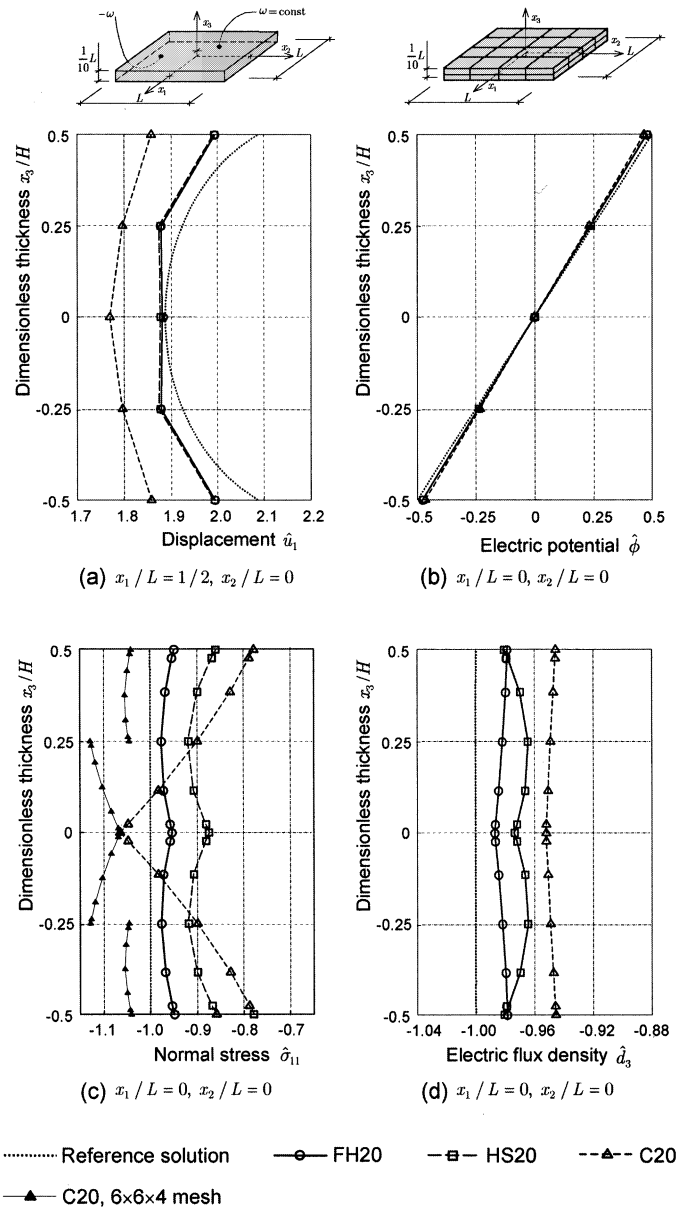


Fig. 7. Case 2, $H/L = 1/10$: (a) normalized displacement $\hat{u}_1$, (b) normalized electric potential $\hat{\phi}$, (c) normalized normal stress $\hat{\sigma}_{11}$ and (d) normalized electric flux density $\hat{d}_3$ in the thickness direction.

## Acknowledgements

The financial support of the (Italian) Ministry for University and Scientific and Technological Research (MURST) made this work possible. Numerical developments were performed at Laboratorio di Meccanica Computazionale (LAMC), DISTART, Università di Bologna, Bologna, Italy.

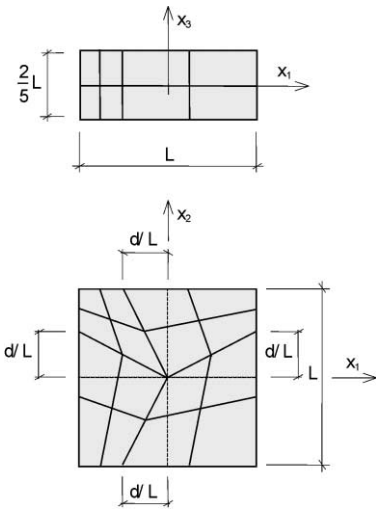


Fig. 8. Distorted mesh scheme.

## Appendix A. Fully hybrid model

(I) In matrix notation, tensor **H** is represented by a $6 \times 6$ matrix, tensor **X** by a $3 \times 3$ matrix and tensor **h** by a $3 \times 6$ matrix. The expressions of matrices and vectors in Eq. (64) are

$$\mathbf{H}_s = \int_{B_e} \mathbf{P}_s^{\mathrm{t}} \mathbf{H} \mathbf{P}_s \, \mathrm{d}V, \quad \mathbf{H}_d = \int_{B_e} \mathbf{P}_d^{\mathrm{t}} \mathbf{X} \mathbf{P}_d \, \mathrm{d}V, \quad \mathbf{H}_{sd} = \int_{B_e} \mathbf{P}_s^{\mathrm{t}} \mathbf{h}^{\mathrm{t}} \mathbf{P}_d \, \mathrm{d}V,$$

$$\mathbf{G}_s = \int_{\partial B_e} \mathbf{L}_u^{\mathrm{t}} \mathbf{N}^{\mathrm{t}} \mathbf{P}_s \, \mathrm{d}S, \quad \mathbf{G}_d = \int_{B_e} \mathbf{L}_\phi^{\mathrm{t}} \mathbf{n}^{\mathrm{t}} \mathbf{P}_d \, \mathrm{d}S,$$

$$\mathbf{g}_s = -\int_{B_e} \mathbf{P}_s^{\mathrm{t}} \mathbf{H} \bar{\mathbf{P}}_s \, \mathrm{d}V \bar{\beta}_s - \int_{B_e} \mathbf{P}_s^{\mathrm{t}} \mathbf{h}^{\mathrm{t}} \bar{\mathbf{P}}_d \, \mathrm{d}V \bar{\beta}_d, \quad \mathbf{g}_u = \int_{\partial B_e} \mathbf{L}_u^{\mathrm{t}} \mathbf{N}^{\mathrm{t}} \bar{\mathbf{P}}_s \, \mathrm{d}S \bar{\beta}_s,$$

$$\mathbf{g}_d = \int_{B_e} \mathbf{P}_d^{\mathrm{t}} \mathbf{X} \bar{\mathbf{P}}_d \, \mathrm{d}V \bar{\beta}_d - \int_{B_e} \mathbf{P}_d^{\mathrm{t}} \mathbf{h} \bar{\mathbf{P}}_s \, \mathrm{d}V \bar{\beta}_s, \quad \mathbf{g}_\phi = -\int_{\partial B_e} \mathbf{L}_\phi^{\mathrm{t}} \mathbf{n}^{\mathrm{t}} \bar{\mathbf{P}}_d \, \mathrm{d}S \bar{\beta}_d,$$

$$\mathbf{h}_u = \int_{\partial B_e} \mathbf{L}_u^{\mathrm{t}} \mathbf{t} \, \mathrm{d}S, \quad \mathbf{h}_\phi = \int_{\partial B_e} \mathbf{L}_\phi^{\mathrm{t}} d \, \mathrm{d}S,$$

where **N** is the matrix containing the direction cosines of the outward normal to $\partial B_e$, and superscript (t) denotes the matrix and vector transpose.

(II) The expressions of matrices and vectors in Eq. (65) are

$$\mathbf{K}_u = \mathbf{G}_s \mathbf{M}^{-1} \mathbf{G}_s^{\mathrm{t}}, \quad \mathbf{K}_\phi = \mathbf{G}_d \left( \mathbf{H}_d^{-1} - \mathbf{H}_d^{-1} \mathbf{H}_{sd}^{\mathrm{t}} \mathbf{M}^{-1} \mathbf{H}_{sd} \mathbf{H}_d^{-1} \right) \mathbf{G}_d^{\mathrm{t}},$$

$$\mathbf{K}_{u\phi} = \mathbf{G}_d \mathbf{H}_d^{-1} \mathbf{H}_{sd}^{\mathrm{t}} \mathbf{M}^{-1} \mathbf{G}_s^{\mathrm{t}},$$

$$\mathbf{f}_u = \mathbf{g}_u + \mathbf{G}_s \mathbf{M}^{-1} \left( \mathbf{g}_s - \mathbf{H}_{sd} \mathbf{H}_d^{-1} \mathbf{g}_d \right),$$

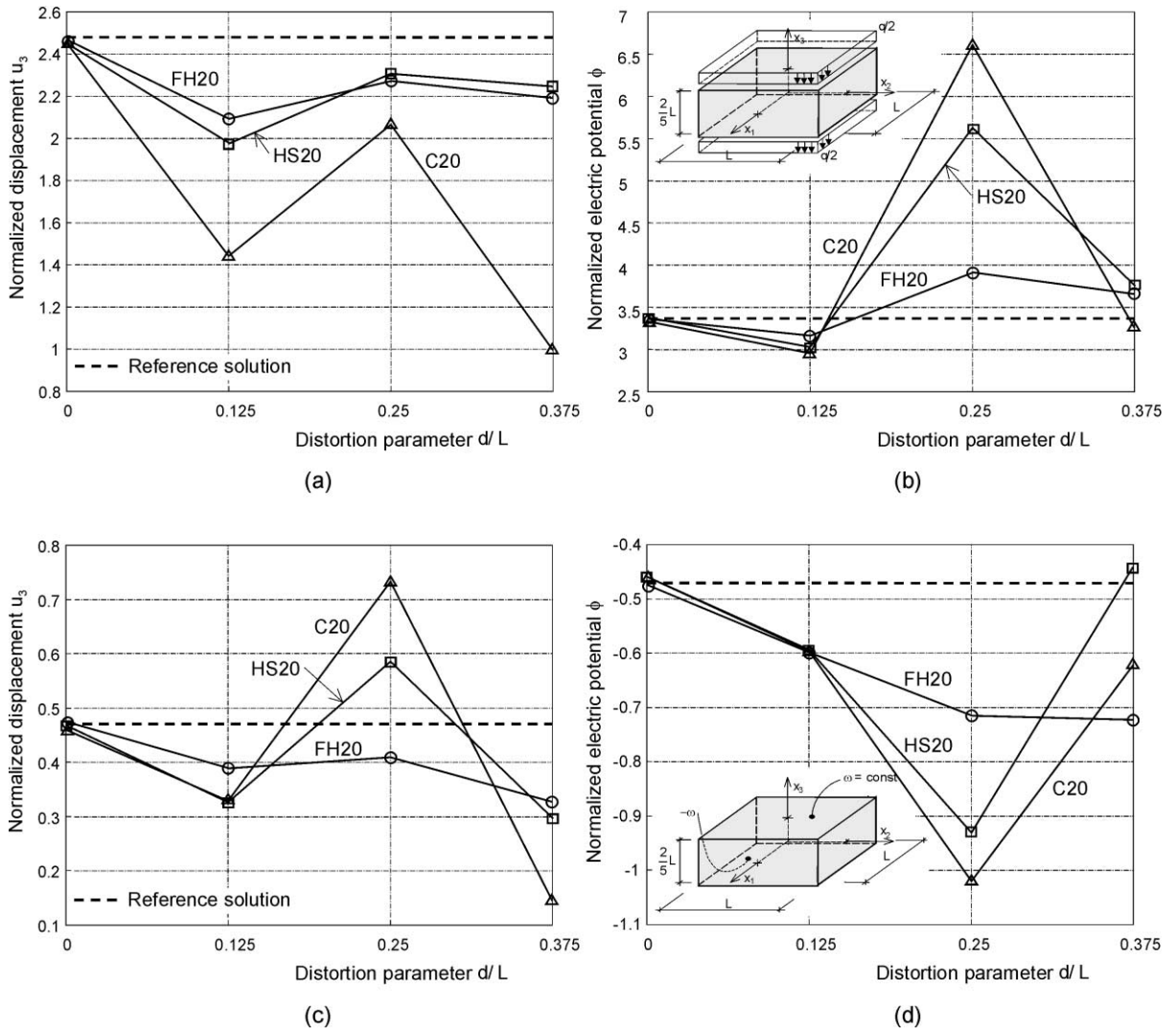


Fig. 9. Sensitivity to element geometry distortion, $H/L = 2/5$. Case 1: (a) normalized displacement $\hat{u}_3$ and (b) normalized electric potential $\hat{\phi}$ at the center of the plate. Case 2: (c) normalized displacement $\hat{u}_3$ and (d) normalized electric potential $\hat{\phi}$ at the center of the bottom face.

$$\mathbf{f}_\phi = \mathbf{g}_\phi - \mathbf{G}_d\mathbf{H}_d^{-1}\left[\left(\mathbf{I} - \mathbf{H}_{sd}^{\mathrm{t}}\mathbf{M}^{-1}\mathbf{H}_{sd}\mathbf{H}_d^{-1}\right)\mathbf{g}_d + \mathbf{H}_{sd}^{\mathrm{t}}\mathbf{M}^{-1}\mathbf{g}_s\right],$$

where

$$\mathbf{M} = \left(\mathbf{H}_s + \mathbf{H}_{sd}\mathbf{H}_d^{-1}\mathbf{H}_{sd}^{\mathrm{t}}\right).$$

## Appendix B. Hybrid stress model

(I) In matrix notation, tensor $\mathbf{H}^e$ is represented by a $6 \times 6$ matrix, tensor $\mathbf{k}^s$ by a $3 \times 3$ matrix and tensor $\mathbf{g}$ by a $3 \times 6$ matrix. The expressions of matrices and vectors in Eq. (67) are

$$\mathbf{H}_s = \int_{B_e} \mathbf{P}_s^{\mathrm{t}} \mathbf{H}^e \mathbf{P}_s \, \mathrm{d}V, \qquad \mathbf{G}_s = \int_{\partial B_e} \mathbf{L}_u^{\mathrm{t}} \mathbf{N}^{\mathrm{t}} \mathbf{P}_s \, \mathrm{d}S, \qquad \mathbf{g}_s = -\int_{B_e} \mathbf{P}_s^{\mathrm{t}} \mathbf{H}^e \bar{\mathbf{P}}_s \, \mathrm{d}V \, \bar{\beta}_s,$$

$$\mathbf{W}_\phi = \int_{B_e} \left(\operatorname{grad} \mathbf{L}_\phi\right)^{\mathrm{t}} \mathbf{k}^s \left(\operatorname{grad} \mathbf{L}_\phi\right) \mathrm{d}V, \qquad \mathbf{W}_{s\phi} = \int_{B_e} \left(\operatorname{grad} \mathbf{L}_\phi\right)^{\mathrm{t}} \mathbf{g} \mathbf{P}_s \, \mathrm{d}V,$$

$$\mathbf{g}_\phi = -\int_{B_e} \mathbf{L}_\phi^{\mathrm{t}} \gamma \, \mathrm{d}V - \int_{B_e} \left(\operatorname{grad} \mathbf{L}_\phi\right)^{\mathrm{t}} \mathbf{g} \bar{\mathbf{P}}_s \, \mathrm{d}V \, \bar{\beta}_s, \qquad \mathbf{g}_u = \int_{\partial B_e} \mathbf{L}_u^{\mathrm{t}} \mathbf{N}^{\mathrm{t}} \bar{\mathbf{P}}_s \, \mathrm{d}V \, \bar{\beta}_s,$$

$$\mathbf{h}_u = \int_{\partial B_e} \mathbf{L}_u^{\mathrm{t}} \mathbf{t} \, \mathrm{d}S, \qquad \mathbf{h}_\phi = \int_{\partial B_e} \mathbf{L}_\phi^{\mathrm{t}} d \, \mathrm{d}S,$$

where $\mathbf{N}$ is the matrix containing the direction cosines of the outward normal to $\partial B_e$, and the superscript (t) denotes the matrix and vector transpose.

(II) The expressions of matrices and vectors resulting from the hybrid stress model in Eq. (65) are

$$\mathbf{K}_u = \mathbf{G}_s \mathbf{H}_s^{-1} \mathbf{G}_s^{\mathrm{t}}, \qquad \mathbf{K}_\phi = \mathbf{W}_\phi - \mathbf{W}_{s\phi} \mathbf{H}_s^{-1} \mathbf{W}_{s\phi}^{\mathrm{t}}, \qquad \mathbf{K}_{u\phi} = \mathbf{W}_{s\phi} \mathbf{H}_s^{-1} \mathbf{G}_s^{\mathrm{t}},$$

$$\mathbf{f}_u = \mathbf{g}_u + \mathbf{G}_s \mathbf{H}_s^{-1} \mathbf{g}_s, \qquad \mathbf{f}_\phi = \mathbf{g}_\phi - \mathbf{W}_{s\phi} \mathbf{H}_s^{-1} \mathbf{g}_s.$$

## Appendix C

Dimensionless quantities in the case of the plate subjected to surface forces:

$$\hat{u}_3 = \frac{\pi^4 H^3 C}{3L^4 q} u_3, \quad \hat{\phi} = \frac{2\pi^2 H \epsilon C}{L^2 F q} \phi, \quad \hat{\sigma}_{11} = \frac{\pi^2 H^2 C}{6(C - C_{66}) L^2 q} \sigma_{11}, \quad \hat{d}_1 = \frac{\pi H C}{N L q} d_1.$$

Dimensionless quantities in the case of the plate subjected to surface electric charges:

$$\hat{u}_1 = \frac{2\pi \epsilon C}{LF\omega} u_1, \quad \hat{\phi} = \frac{\epsilon C}{HG\omega} \phi, \quad \hat{\sigma}_{11} = \frac{\epsilon C}{F C_{66} \omega} \sigma_{11}, \quad \hat{d}_3 = \frac{1}{\omega} d_3.$$

Auxiliary constants:

$$C = C_{11} - \frac{k_{33} C_{13}^2 + 2 c_{31} c_{33} C_{13} - c_{31}^2 C_{33}}{k_{33} C_{33} + c_{33}^2}, \qquad \epsilon = k_{11} + \frac{c_{15}^2}{C_{44}},$$

$$F = \epsilon \frac{c_{33} C_{13} - c_{31} C_{33}}{k_{33} C_{33} + c_{33}^2}, \qquad N = \frac{c_{15} C - C_{44} F}{C_{44}}, \qquad G = \epsilon \frac{C_{11} C_{33} - C_{13}^2}{k_{33} C_{33} + c_{33}^2}.$$

## References

Allik, H., Hughes, T.J.R., 1970. Finite element method for piezoelectric vibration. Int. J. Num. Meth. Engng. 2, 151–157.

Berlincourt, D.A., Curran, D.R., Jaffe, H., 1964. Piezoelectric and Piezomagnetic Materials and their Functions as Transducers. In: Mason, W.P. (Ed.), Physical Acoustics, IA, Academic Press, New York, pp. 170–267.

Bisegna, P., Maceri, F., 1996. An exact three-dimensional solution for simply supported rectangular piezoelectric plates. J. Appl. Mech. 63, 628–638.

Bisegna, P., Maceri, F., 1998. Twenty-five functionals of linear piezoelectricity. Internal Report 51, Department of Civil Engineering, University of Rome "Tor Vergata", Italy.

Brezzi, F., Fortin, M., 1991. Mixed and Hybrid Finite Element Methods. Springer, New York.

Cannarozzi, A.A., Ubertini, F., 1999. Un approccio variazionale ibrido in elettroelasticità (in Italian). In: Proc. XII Convegno Italiano di Meccanica Computazionale - GIMC, Napoli, Italy, pp. 29–36. Publication no. 82, 1999, DISTART, University of Bologna, Italy.

Carotenuto, R., Lamberti, N., Iula, A., Pappalardo, M., 1998. A new low voltage piezoelectric micromotor based on stator precessional motion. IEEE Trans. Ultrason., Ferroelect., Freq. Contr. 45, 1427–1435.

dell'Isola, F., Vidoli, S., 1998. Continuum modelling of piezoelectromechanical truss beams: an application to vibration damping. Arch. Appl. Mech. 68, 1–19.

EerNisse, E.P., 1967. Variational method for electroelastic vibration analysis. IEEE Trans. Sonics Ultrason. SU-14, 153–160.

Eringen, A.C., Maugin, G.A., 1990. Electrodynamics of Continua I. Foundations and Solid Media. Springer, New York.

Gandhi, M.V., Thompson, B.S., 1992. Smart Materials and Structures. Chapman & Hall, London.

Heyliger, P., 1994. Static behavior of laminated elastic/piezoelectric plates. AIAA J. 32, 2481–2484.

Heyliger, P., 1997. A note on the static behavior of simply-supported laminated piezoelectric cylinders. Int. J. Solids Struct. 34, 3781–3794.

Holland, R., EerNisse, E.P., 1968. Variational evaluation of admittances of multielectroded three-dimensional piezoelectric structures. IEEE Trans. Sonics Ultrason. SU-15, 119–132.

Ikeda, T., 1996. Fundamentals of Piezoelectricity. Oxford University Press, Oxford.

Kapuria, S., Sengupta, S., Dumir, P.C., 1997. Three-dimensional solution for simply-supported piezoelectric cylindrical shell for axisymmetric load. Comput. Meth. Appl. Mech. Engng. 140, 139–155.

Lee, H.-J., Saravanos, D.A., 1997. Generalized finite element formulation for smart multilayered thermal piezoelectric composite plates. Int. J. Solids Struct. 34, 3355–3371.

Lerch, R., 1990. Simulation of piezoelectric devices by two- and three-dimensional finite elements. IEEE Trans. Ultrason. Ferroelect. Freq. Contr. 37, 233–247.

Nicotra, V., 1998. Piastre elettroelastiche capaci di vibrazioni di spessore. Ph.D. Dissertation, University of Roma "Tor Vergata", Italy.

Nicotra, V., Podio Guidugli, P., 1998. Piezoelectric plates with changing thickness. J. Struct. Cont. 5, 73–86.

Oden, J.T., Kelley, B.E., 1971. Finite element formulation of general electrothermoelasticity problems. Int. J. Num. Meth. Engng. 3, 161–179.

Pian, T.H.H., 1973. Hybrid models. In: Fenves, S.J., Perrone, R., Robinson R., Schonbrich, W.C. (Eds.), Numerical and Computer Methods in Structural Mechanics. Academic Press, New York, pp. 50–80.

Ray, M.C., Rao, K.M., Samanta, B., 1992. Exact analysis of coupled electroelastic behaviour of a piezoelectric plate under cylindrical bending. Comput. Struct. 45, 667–677.

Ray, M.C., Bhattacharya, R., Samanta, B., 1993. Exact solutions for static analysis of intelligent structures. AIAA J. 31, 1684–1691.

Sewell, M.J., 1987. Maximum and Minimum Principles. Cambridge University Press, Cambridge.

Sze, K.Y., Chow, C.L., Wanji, C., 1992. On invariance of isoparametric hybrid/mixed elements. Comm. Appl. Numer. Meth. 8, 385–406.

Tiersten, H.F., 1967. Hamilton's principle for linear piezoelectric media. Proceedings of the IEEE, 1523–1524.

Tiersten, H.F., 1969. Linear Piezoelectric Plate Vibrations. Plenum Press, New York.

Vidoli, S., Batra, R.C., 1998. Derivation of plate and beam equations for a piezoelectric body from a mixed three-dimensional variational principle. J. Elasticity, submitted for publication.

Voigt, W., 1910. Leherbuch der Kristallphysik. Leipzig.

Wang, J., Yong, Y.-K., Imai, T., 1999. Finite element analysis of the piezoelectric vibrations of quartz plate resonators with higher-order plate theory. Int. J. Solids Struct. 36, 2303–2319.

Yang, J.S., 1992. Mixed variational principles for piezoelectric elasticity. In: Antar, B., Engels, R., Prinaris, A.A., Moulden, T.H. (Eds.), Developments in Theoretical and Applied Mechanics, XVI, II.1.31-38, University of Tennessee Space Institute, Tennessee.

Zanaboni, O., 1936. Il problema della funzione delle tensioni in un sistema spaziale isotropo. Bollettino U.M.I., XV, 2, 71–76.

Zhang, H.-L., 1985. On variational principles of a piezoelectric body. (in Chinese) Acta Acoustica 10, 223–230.

Zienkiewicz, O.C., Taylor, R.L.T., 1989. The Finite Element Method. McGraw-Hill, London.